Article

Cell Reports

Reduced peroxisomal import triggers peroxisomal retrograde signaling

Graphical Abstract

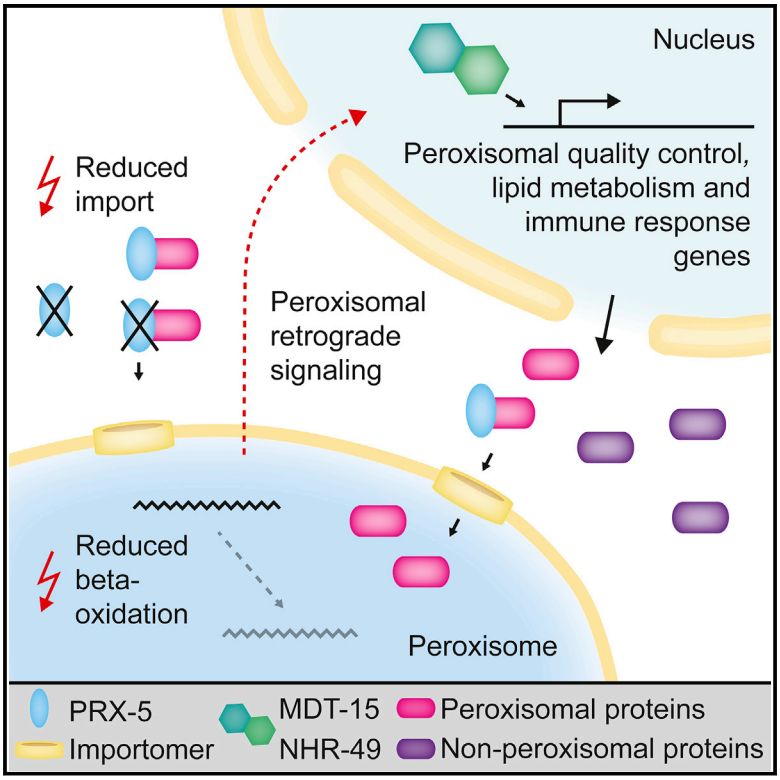

Authors

Elisabeth Rackles, Michael Witting, Ignasi Forné, ..., Christof Osman, Axel Imhof, Stéphane G. Rolland

Correspondence

srolland@ibs.re.kr

In Brief

Retrograde signaling pathways have been identified for several organelles. Rackles et al. identify an analogous mechanism for peroxisomes in *Caenorhabditis elegans*. They propose that it plays a role in maintenance of lipid homeostasis and may act as a surveillance mechanism against pathogen infection.

Highlights

- Peroxisomal import stress induces peroxisomal retrograde signaling (PRS)
- PRS requires the transcription factors NHR-49/PPARα and MDT-15/MED15
- PRS target genes act in peroxisome quality control, lipid metabolism, and immunity

Rackles et al., 2021, Cell Reports *34*, 108653
January 19, 2021
https://doi.org/10.1016/j.celrep.2020.108653

CellPress

Cell Reports

CellPress
OPEN ACCESS

Article

Reduced peroxisomal import triggers peroxisomal retrograde signaling

Elisabeth Rackles,[1] Michael Witting,[4,5] Ignasi Forné,[2] Xing Zhang,[3] Judith Zacherl,[1] Simon Schrott,[1] Christian Fischer,[1] Jonathan J. Ewbank,[3] Christof Osman,[1] Axel Imhof,[2] and Stéphane G. Rolland[1,6,7,*]

[1]Faculty of Biology, Ludwig Maximilian University of Munich, 82152 Martinsried, Germany
[2]Protein Analysis Unit, BioMedical Center, Faculty of Medicine, Ludwig Maximilian University of Munich, Großhadernerstr. 9, 82152 Martinsried, Germany
[3]Aix Marseille Univ, CNRS, INSERM, CIML, Turing Centre for Living Systems, Marseille, France
[4]Research Unit Analytical BioGeoChemistry, Helmholtz Zentrum München, Ingolstädter Landstraße 1, 85764 Neuherberg, Germany
[5]Chair of Analytical Food Chemistry, TUM School of Life Sciences, Technical University of Munich, Maximus-von-Imhof-Forum 2, 85354 Freising, Germany
[6]Present address: Center for Genomic Integrity, Institute for Basic Science (IBS), Ulsan 44919, South Korea
[7]Lead contact
*Correspondence: srolland@ibs.re.kr
https://doi.org/10.1016/j.celrep.2020.108653

SUMMARY

Maintaining organelle function in the face of stress is known to involve organelle-specific retrograde signaling. Using *Caenorhabditis elegans*, we present evidence of the existence of such retrograde signaling for peroxisomes, which we define as the peroxisomal retrograde signaling (PRS). Specifically, we show that peroxisomal import stress caused by knockdown of the peroxisomal matrix import receptor *prx-5/PEX5* triggers NHR-49/peroxisome proliferator activated receptor alpha (PPARα)- and MDT-15/MED15-dependent upregulation of the peroxisomal Lon protease *lonp-2/LONP2* and the peroxisomal catalase *ctl-2/CAT*. Using proteomic and transcriptomic analyses, we show that proteins involved in peroxisomal lipid metabolism and immunity are also upregulated upon *prx-5(RNAi)*. While the PRS can be triggered by perturbation of peroxisomal β-oxidation, we also observed hallmarks of PRS activation upon infection with *Pseudomonas aeruginosa*. We propose that the PRS, in addition to a role in lipid metabolism homeostasis, may act as a surveillance mechanism to protect against pathogens.

INTRODUCTION

Various human diseases, for example Refsum's disease or X-linked adrenoleukodystrophy, are associated with disrupted fatty acid metabolism. The degradation of long-chain and very-long-chain fatty acids takes place by β-oxidation in peroxisomes. Consequently, impaired peroxisomal function leads to perturbation of fatty acid metabolism (Van Veldhoven, 2010). Studying how the function of peroxisomes is maintained in response to stress can contribute to our understanding of metabolic disorders.

One cycle of peroxisomal β-oxidation reduces a fatty acid chain by two carbon atoms and leads to release of one acetyl-CoA molecule in a four-step enzymatic reaction (Van Veldhoven, 2010). The enzymes involved in this shortening of fatty acids are conserved from mammals to *C. elegans*. In *C. elegans*, the peroxisomal β-oxidation pathway has mainly been studied in the context of ascaroside pheromone biosynthesis (Butcher et al., 2007; Golden and Riddle, 1982; Srinivasan et al., 2008, 2012; von Reuss et al., 2012). However, peroxisomal β-oxidation enzymes have also been proposed to play a role in general β-oxidation of fatty acids (Artyukhin et al., 2018; Van Gilst et al., 2005; Zhang et al., 2010).

In mammals, peroxisomal lipid metabolism is regulated by peroxisome proliferator activated receptor alpha (PPARα). PPARα can be activated by a broad spectrum of ligands, including natural (e.g., fatty acids) and synthetic compounds (i.e., peroxisome proliferators) (Viswakarma et al., 2010). In *C. elegans*, the nuclear hormone receptor NHR-49 has been proposed to be the functional homolog of PPARα (Van Gilst et al., 2005). It regulates specific lipid metabolic pathways by forming heterodimers with different co-factors (such as MDT-15, the homolog of human Mediator MED15) (Pathare et al., 2012). For example, the NHR-49/MDT-15 heterodimer has been shown to control genes encoding fatty acid desaturases and genes involved in the fasting response (Taubert et al., 2006).

The proteins involved in peroxisomal biogenesis are called peroxins. In mammals, they are encoded by *PEX* genes. Mature peroxisomes import folded peroxisomal matrix proteins and also protein complexes. Peroxisomal matrix proteins are recognized through their C-terminal peroxisomal targeting signal 1 (PTS1) by the cytosolic receptor PEX5 (Francisco et al., 2017). Grafting a PTS1 onto a cytoplasmic protein is sufficient to drive peroxisomal import. The importance of functional import of peroxisomal matrix proteins by PEX5 is highlighted by severe disorders

caused by *PEX5* mutations (Wiemer et al., 1995). A few proteins contain an N-terminal PTS2 signal that is recognized by the receptor PEX7 (Francisco et al., 2017). In *C. elegans*, peroxins are encoded by *prx* genes, and homologs of 11 of the 14 human peroxins have been identified (Petriv et al., 2002; Thieringer et al., 2003). The PTS2-targeting pathway is absent from *C. elegans* (Motley et al., 2000), and all peroxisomal proteins are imported by PRX-5, the homolog of human PEX5 (Gurvitz et al., 2000; Petriv et al., 2002).

Organelle-specific retrograde signaling pathways have been shown to be activated in response to disruption of protein homeostasis in mitochondria or the endoplasmic reticulum. These so-called unfolded protein responses (UPRs) lead to transcriptional upregulation of effector genes encoding organelle-specific proteins (such as proteases, chaperones, and detoxifying enzymes), which participate in organelle quality control and maintenance of organelle function (Pellegrino et al., 2013; Sasaki and Yoshida, 2015). There have been hints that such retrograde signaling might exist for peroxisomes. For example, the peroxisomal Lon protease has been shown to degrade misfolded peroxisomal matrix proteins *in vivo* (Aksam et al., 2007; Bartoszewska et al., 2012) and to have chaperone activity *in vitro* (Bartoszewska et al., 2012) and therefore might act in a manner analogous to the mitochondrial Lon protease in the mitochondrial UPR (UPR^{mt}).

In this study, we present evidence that peroxisomal retrograde signaling (PRS) exists in *C. elegans* and is activated in response to peroxisomal import stress caused by diminution of peroxisomal matrix protein import following knockdown of *prx-5*/*PEX5*. Specifically, we found that peroxisomal import stress triggers transcriptional upregulation of the peroxisomal Lon protease *lonp-2*/*LONP2* and catalase *ctl-2*/*CAT* in a manner dependent on NHR-49/PPARα and its co-factor MDT-15/MED15. Lipidomic analysis revealed that *prx-5(RNAi)* animals have increased levels of triacylglycerols with longer acyl chains that normally would be catabolized by peroxisomal β-oxidation. The presence of excess long-chain fatty acids could be the signal that activates the PRS. Consistent with this hypothesis, we found that directly perturbing peroxisomal β-oxidation is sufficient to activate the PRS. Using transcriptomics and proteomics approaches, we found that peroxisomal import stress also induces upregulation of peroxisomal lipid metabolism, which could be a mechanism to cope with reduced β-oxidation. Additionally, proteins involved in the immune response are upregulated, and we observed hallmarks of PRS activation upon infection with *Pseudomonas aeruginosa*. Thus, the PRS may fulfill two functions: maintaining the homeostasis of lipid metabolism and acting as a potential surveillance mechanism to protect against pathogens.

RESULTS

Diminished peroxisomal matrix protein import induces the transcriptional upregulation of the peroxisomal Lon protease *lonp-2/LONP2* and the peroxisomal catalase *ctl-2/CAT*

The UPR^{mt} is induced by perturbation of mitochondrial protein import (Nargund et al., 2012). We wondered whether a potential PRS would be triggered by diminution of peroxisomal matrix protein import. To monitor *C. elegans* peroxisomal matrix protein import, we generated a strain co-expressing a reporter of the peroxisomal membrane (GFP::PXMP-4) and a reporter of active peroxisomal import (mKate2::DAF-22). PXMP-4 is a homolog of the human peroxisomal membrane protein PXMP4 (Pinto et al., 2006), and DAF-22 is a β-oxidation enzyme that localizes to the peroxisomal matrix through its PTS1 sequence (Butcher et al., 2009; Figure 1A). Both constructs were placed under control of the *daf-22* promoter, which drives expression in the intestine, epidermis, and body wall muscle cells (Butcher et al., 2009). Analysis of a strain carrying both reporters as single-copy MosSCI insertions (Mos1-mediated single-copy insertion; Frøkjær-Jensen et al., 2012) revealed punctate, mostly overlapping signals characteristic of peroxisomes (Figure 1B).

When we knocked down the gene encoding the peroxisomal import receptor PRX-5, we observed complete or partial block of mKate2::DAF-22 import into peroxisomes of intestinal cells in almost all animals analyzed (91%; Figures 1B, 1C, S1A, and S1B). In contrast, its import did not seem to be affected in the epidermis (Figure 1B). Because the signal intensity of this reporter strain was too weak to allow quantitative analysis, we instead used a multi-copy reporter strain expressing GFP::PTS1 and mKate2::PXMP-4 under control of the epidermis-specific *vha-7* promoter (Figure 1D). *prx-5(RNAi)* did not significantly change the number of GFP::PTS1-labeled peroxisomes. In contrast, the number of mKate2::PXMP-4-labeled peroxisomes increased 1.7-fold upon *prx-5(RNAi)* (Figure 1E). Although most of the GFP and mKate2 signals co-localized in *control(RNAi)* animals, an increased number of mKate2-labeled peroxisomes that were not labeled with GFP were visible in *prx-5(RNAi)* animals (Figures S1C and S1D). Because we did not observe an obvious increase in cytoplasmic GFP signal, it remains unclear whether these peroxisomal structures are peroxisomes that are import incompetent, pre-peroxisomal vesicles that would be also import incompetent, or peroxisomes undergoing pexophagy. Parenthetically, mKate2 is less pH sensitive than GFP (Botman et al., 2019). Thus, peroxisomes undergoing pexophagy would still exhibit some mKate2 fluorescence but no GFP fluorescence because GFP would be quenched by the acidic pH of the autophagolysosomes. Hence, under our RNAi conditions, *prx-5* knockdown leads to a partial block in peroxisomal matrix protein import in intestinal cells (and compromised peroxisome homeostasis in epidermal cells). In the following experiments, we examined the cellular response to *prx-5* knockdown-induced peroxisomal import stress.

To investigate whether retrograde signaling exists for peroxisomes, we generated a transcriptional reporter to monitor the expression of *lonp-2* (*lonp-2p::GFP*). *lonp-2* encodes the homolog of the human Lon protease LONP2 and, like LONP2, localizes to peroxisomes (Figure S2). We also generated a transcriptional reporter to monitor the expression of *C. elegans* catalase genes. *C. elegans* has three catalase genes in a tandem array (*ctl-3*, *ctl-1*, and *ctl-2*). Only *ctl-2* encodes a protein with a PTS1, the homolog of human peroxisomal catalase CAT. Because the sequences of the promoters of *ctl-2* and *ctl-1* are identical, this reporter also monitors the expression of *ctl-1,* but we refer to it here as *ctl-2p::GFP* for simplicity. We tested the effect of *prx-5(RNAi)*

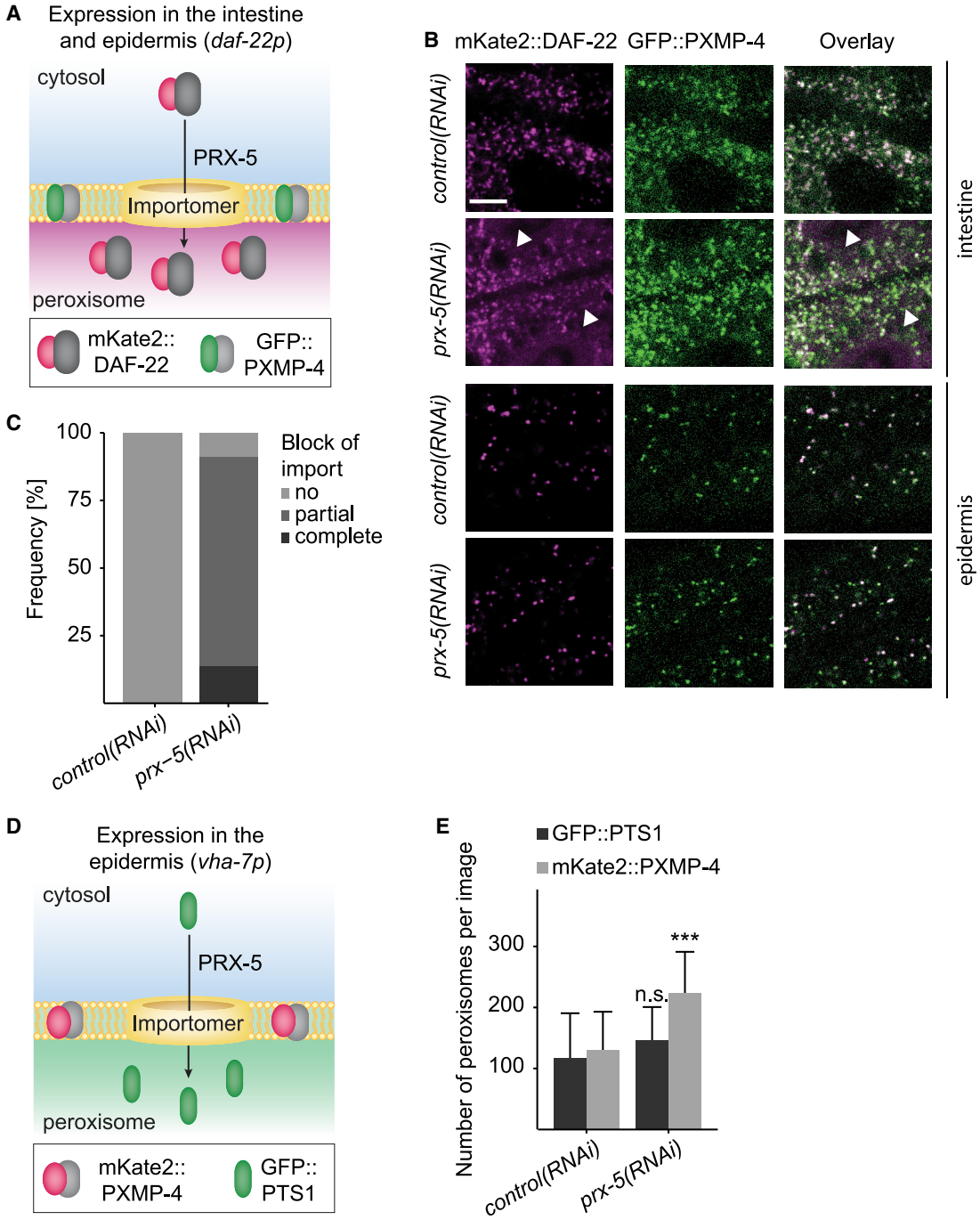

Figure 1. Inactivation of *prx-5* leads to a reduction in peroxisomal matrix protein import in the intestine

(A) Schematic representation of the *daf-22p::mKate2::daf-22* and *daf-22p::gfp::pxmp-4* reporters used in the study.

(B) L4 larvae carrying the *daf-22p::mKate2::daf-22* and *daf-22p::gfp::pxmp-4* reporters were subjected to *prx-5(RNAi)* or *control(RNAi).* Adults of the next generation were analyzed by confocal microscopy. Shown are representative images of a worm showing partial block of mKate2::DAF-22 import in the intestine upon *prx-5(RNAi)* (top panels) and no block in the epidermis (bottom panels). Scale bar, 5 μm. Arrowheads, region with cytoplasmic mKate2::DAF-22 signal.

(C) Semiquantitative analysis of mKate2::DAF-22 import upon *prx-5(RNAi)* in intestinal cells. n = 22 (n = number of animals analyzed). Complete block, the mKate2::DAF-22 signal appears solely cytosolic; partial block, the mKate2::DAF-22 signal is partially cytosolic and peroxisomal.

(D) Schematic representation of the *vha-7p::GFP::PTS1* and *vha-7p::mKate2::pxmp-4* reporters used in the study.

(E) The number of peroxisomes per image was quantified in the GFP or mKate2 channel. n = 15–20 animals analyzed. Mean and SD are shown. For GFP, ns = not significant by Mann-Whitney *U* test to *control(RNAi).* For mKate2, ***p < 0.001 by two-sample t test to *control(RNAi).*

See also Figure S1.

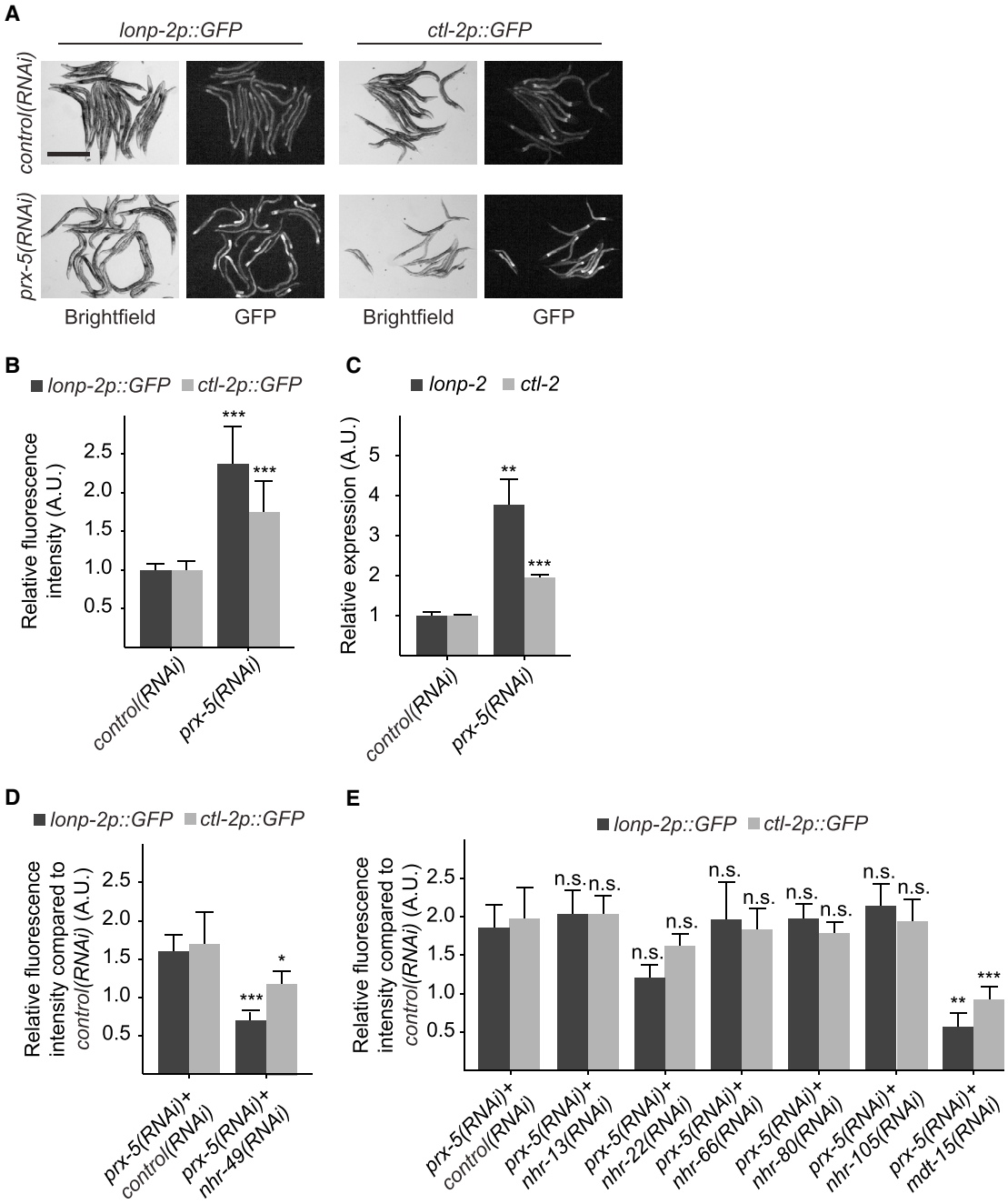

Figure 2. Inactivation of *prx-5* leads to NHR-49/MDT-15-dependent upregulation of *lonp-2* and *ctl-2*

(A) L4 larvae carrying the *lonp-2p::GFP* or *ctl-2p::GFP* reporter were subjected to *prx-5(RNAi)*. Adults of the next generation were analyzed by bright-field and fluorescence microscopy. Scale bar, 0.5 mm. Images were scaled with a minimum displayed value of 0 and a maximum displayed value that equals the maximum pixel value of the control. Although rescaling enhanced the signal, some pixels of the images are saturated. For details, see STAR methods. For unsaturated images, see Figure S3.

(B) Quantification of the fluorescence intensity relative to the *control(RNAi)*. It should be noted that, although we measured the GFP level in the entire animal, the reporters are mostly expressed in intestinal cells. Mean and SD are shown; n = 7 biological replicates for *lonp-2p::GFP* and ***p < 0.001 by Welch two-sample t test to *control(RNAi)*; n = 10 biological replicates for *ctl-2p::GFP* and ***p < 0.001 by two-sample t test to *control(RNAi)*.

(C) RT-qPCR analysis of *lonp-2* and *ctl-2* expression. Wild-type L4 larvae were subjected to *prx-5(RNAi)*, and adults of the next generation were analyzed. Mean and SD are shown; n = 3 biological replicates; **p < 0.01 and ***p < 0.001 by two-sample t test to *control(RNAi)*.

(D) Analysis of the role of NHR-49 in the PRS. *prx-5(RNAi)* was diluted 1:2 with *control(RNAi)* or *nhr-49(RNAi)*. n = 6 biological replicates; mean and SD are shown; *p < 0.5 and ***p < 0.001 by two-sample t test to the control *prx-5(RNAi) + control(RNAi)*.

(legend continued on next page)

on the expression of *lonp-2p::GFP* and *ctl-2p::GFP*. *prx-5(RNAi)* caused 2.4- and 1.7-fold upregulation of *lonp-2p::GFP* and *ctl-2p::GFP* compared with *control(RNAi)*, respectively (Figures 2A and 2B). These changes correlated with increased *gfp* mRNA levels, as monitored by RT-qPCR (Figure S4A). Furthermore, we showed that, in wild-type N2 animals, *prx-5(RNAi)* caused 3.8- and 1.9-fold upregulation of the endogenous *lonp-2* and *ctl-2* genes, respectively (Figures 2C, S4B, and S4C).

These results indicate that impairing peroxisomal matrix protein import by knocking down *prx-5* induces transcriptional upregulation of the peroxisomal Lon protease *lonp-2* and the peroxisomal catalase *ctl-2*, identifying a PRS mechanism in *C. elegans*.

NHR-49/PPARα and its co-activator MDT-15/MED15 act as transcription factors in the PRS

Because the nuclear hormone receptor NHR-49 is required for transcriptional regulation of various peroxisomal pathways (Van Gilst et al., 2005), we tested whether the PRS is dependent on NHR-49. To that end, we knocked down *prx-5* together with *nhr-49* or our control RNAi (Figure 2D). Double RNAi of *prx-5* with the control caused upregulation of *lonp-2p::GFP* and *ctl-2p::GFP*. In contrast, double RNAi of *prx-5* with *nhr-49* resulted in complete suppression of upregulation of both reporters, indicating that the PRS is dependent on NHR-49. In addition, *nhr-49* knockdown in the absence of peroxisomal import stress (*control(RNAi)* + *nhr-49(RNAi)*; Figure S4D) caused decreased expression of *lonp-2p::GFP* but not of *ctl-2p::GFP*. Hence, basal expression of *lonp-2p::GFP* but not *ctl-2p::GFP* is dependent on NHR-49.

Because NHR-49 regulates different metabolic pathways by forming heterodimers with six different co-factors (Pathare et al., 2012), we tested these co-factors for their potential role in the PRS. Only double RNAi of *prx-5* with *mdt-15* resulted in complete suppression of upregulation of both reporters (Figure 2E), indicating that the PRS is dependent on MDT-15. In addition, *mdt-15* knockdown in the absence of peroxisomal import stress (*control(RNAi)* + *mdt-15(RNAi)*; Figure S4D) caused a decrease of the expression of both reporters, indicating that *lonp-2p::GFP* and *ctl-2p::GFP* basal expression is dependent on MDT-15.

Thus, NHR-49/PPARα and its co-factor MDT-15/MED15 are required for induction of the PRS.

Lipidomic analysis indicates a reduction of peroxisomal lipid metabolism in *prx-5(RNAi)* animals

The reduction of peroxisomal matrix protein import by *prx-5(RNAi)* is expected to affect the import of peroxisomal β-oxidation enzymes (Figure 3A). This would reduce peroxisomal β-oxidation and cause accumulation of long-chain fatty acids that fail to be catabolized in peroxisomes. To test this possibility, we analyzed the lipidome of wild-type animals treated with *prx-5(RNAi)* or *control(RNAi)*. We found 241 upregulated and 322 downregulated lipid clusters in *prx-5(RNAi)* (Figure 3B; Table S1). To determine which lipid classes were specifically affected upon *prx-5(RNAi)*, we performed lipid identification based on MS1 annotation and MS2 fragmentation data analysis (MS1, mass spectrometry; MS2, tandem mass spectrometry) and compared results for each individual lipid class. An interesting example is triacylglycerols (TGs). Using the sum of all lipid clusters as a proxy for the total amount of TGs and, therefore, as a proxy for lipid droplet content, no difference was found between *prx-5(RNAi)* and *control(RNAi)* animals. Closer examination showed that, of the total 429 identified TGs, 59 were upregulated and 30 downregulated. Interestingly, upregulated TGs have longer acyl chains, whereas downregulated TGs have short acyl chains (Figure 3C), reflecting a potential decrease of β-oxidation in *prx-5(RNAi)* animals. Peroxisomal β-oxidation is responsible for breaking down long- and odd-chain fatty acids. One specific example is TG(60:2), which was three times more abundant following *prx-5(RNAi)*. Fragmentation spectrum analysis showed that this lipid contains C24:0 and C26:0 acyl groups, which are normally broken down in peroxisomes (Figure 3D). For other lipid classes (such as phosphatidylcholines [PCs] or phosphatidylethanolamines [PEs]), no similar trend in acyl chain length was found (Figure S5). This suggests that membrane lipids can be maintained during peroxisomal dysfunction but that long-chain fatty acids accumulate and are stored as TGs. Ether lipids are another class of lipids that require functional peroxisomes (Drechsler et al., 2016; Shi et al., 2016). Almost all of the detected and identified ether lipids were downregulated (Figure S5). These results indicate that *prx-5(RNAi)* animals exhibit reduced peroxisomal lipid metabolism.

The PRS is specifically activated by a perturbation of peroxisomal β-oxidation in an NHR-49-dependent manner

Decreased β-oxidation upon *prx-5(RNAi)* alters the composition of lipids in the cell. This alteration could be one signal that triggers the PRS. To test this hypothesis, we directly reduced peroxisomal β-oxidation by knocking down the six genes encoding the *C. elegans* acyl-coenzyme A (CoA) oxidases (*acox-1.1–acox-1.6*) and analyzed the expression of *lonp-2p::GFP* and *ctl-2p::GFP*. Knockdown of *acox-1.1* and *acox-1.4* caused a significant upregulation of *lonp-2p::GFP* and *ctl-2p::GFP* expression (Figures 4A and 4B). Moreover, *acox-1.3(RNAi)* caused a significant upregulation of *ctl-2p::GFP* expression. Next we knocked down *maoc-1* and *dhs-28*, which encode functional homologs of the mammalian bi-functional enzyme MFE2 (Butcher et al., 2009; von Reuss et al., 2012; Zhang et al., 2010), as well as *daf-22*, which encodes a homolog of the thiolase domain of human sterol carrier protein X (SCPx) (Butcher et al., 2009). Knockdown of these genes caused an ~2-fold induction of *lonp-2p::GFP* and *ctl-2p::GFP* expression (Figure 4C). We also knocked down the genes encoding ACS-7 and ACOX-3, two enzymes that modify

(E) Analysis of the role of NHR-49 co-factors in the PRS. *prx-5*(*RNAi*) was diluted 1:2 with *control(RNAi)* or RNAi against different NHR-49 co-factors. n = 6–14 biological replicates; mean and SD are shown. For *lonp-2p::GFP*, **p < 0.01 by Kruskal-Wallis test with Dunn's multiple comparisons test. For *ctl-2p::GFP*, ***p < 0.001 by one-way ANOVA with Dunnett's multiple comparisons to the control *prx-5(RNAi)* + *control(RNAi)*.
See also Figures S2–S4.

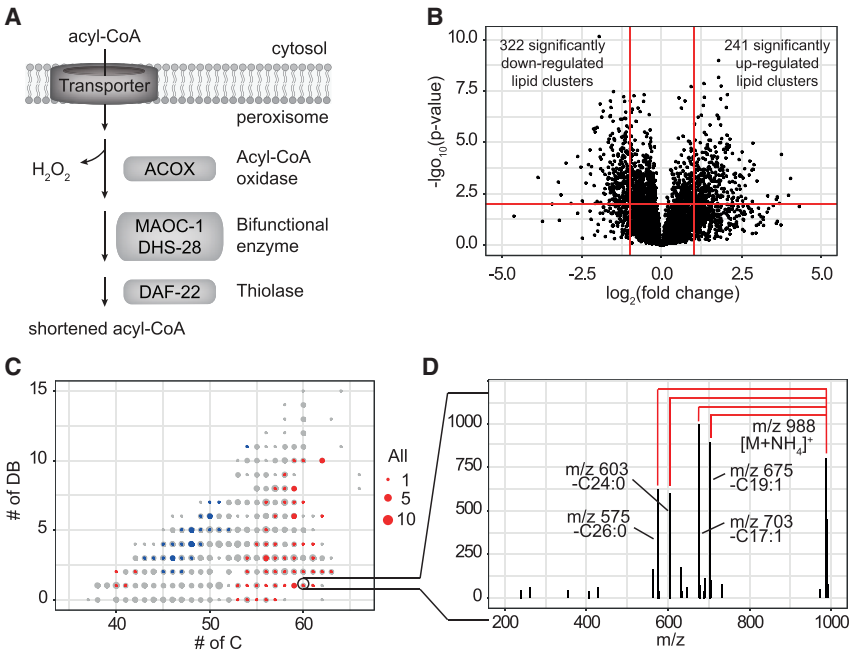

Figure 3. Lipidomics analysis indicates a reduction of peroxisomal lipid metabolism in *prx-5(RNAi)* animals

(A) Schematic of the *C. elegans* peroxisomal β-oxidation pathway.

(B) 6,015 of 7,620 detected lipid clusters passed our QC (quality control) filter and were evaluated further statistically. Lipid clusters with $p < 0.01$ and an absolute fold change of more than 2 were regarded as differentially regulated upon *prx-5(RNAi)*.

(C) Scatterplot indicating the distribution and changes in the levels of TG species in *prx-5(RNAi)* in comparison with *control(RNAi)*. The x axis labels the number of carbons (# of C) and the y axis the number of double bonds (# of DB) in the acyl side chains. Red and blue dots indicate upregulated and downregulated TGs, respectively.

(D) MS^2 spectrum of TG(60:2) as an example of one upregulated TG. Different acyls are detected as neutral loss from the $[M+NH_4]^+$ adduct. Detected fragments indicate that this lipid feature is a mixture of TG(17:1_17:1_26:0) and TG(17:1_19:1_24:0). Both contain saturated long-chain acyls (24:0 and 26:0), which are typically shortened by peroxisomal β-oxidation.

See also Figure S5 and Table S1.

ascarosides, which are also synthesized by peroxisomal β-oxidation (Zhou et al., 2018). *acs-7(RNAi)* and *acox-3(RNAi)* did not result in significant upregulation of *lonp-2p::GFP* and *ctl-2p::GFP* expression (Figure 4C). We also tested whether perturbation of mitochondrial β-oxidation can induce the PRS. To that end, we knocked down *ech-6* and *acdh-13*, which encode two mitochondrial β-oxidation enzymes. Although *ech-6(RNAi)* and *acdh-13(RNAi)* caused strong upregulation of the UPR^{mt} transcriptional reporter *hsp-6p::GFP* (Figure S6A), knockdown of these genes did not significantly affect *lonp-2p::GFP* and *ctl-2p::GFP* expression (Figure S6B). Hence, the PRS is specifically activated by perturbing peroxisomal β-oxidation. Finally, we knocked down *maoc-1* together with *nhr-49* and observed complete suppression of upregulation of both reporters (Figure 4D). In conclusion, the PRS is specifically activated upon perturbation of peroxisomal β-oxidation in an NHR-49-dependent manner.

The PRS is not induced by a redox imbalance between the cytosol and peroxisomes

Peroxisomes play an important role in scavenging reactive oxygen species (ROS). Reduced peroxisomal matrix protein import will result in reduced import of the peroxisomal catalase and, thus, in disruption of the redox balance between the cytosol and peroxisomes. This imbalance might also act as a signal in the PRS. To induce a redox imbalance between the cytosol and peroxisomes, we knocked down the cytosolic catalase *ctl-1* or the peroxisomal catalase *ctl-2* and did not observe any upregulation of *lonp-2p::GFP* and *ctl-2p::GFP* (Figure 5A). Consistent with these results, the *ctl-2(ua90)* loss-of-function mutation (Petriv and Rachubinski, 2004) did not cause upregulation of either reporter (Figures 5B and 5C). This set of experiments indicates that a redox imbalance between peroxisomes and the cytosol does not induce the PRS.

Transcriptomic and proteomic analyses reveal that genes/proteins involved in the immune response and peroxisomal lipid metabolism are upregulated upon activation of the PRS

To identify additional targets of the PRS, the transcriptome and proteome of wild-type animals subjected to *prx-5(RNAi)* or *control(RNAi)* were analyzed by RNA sequencing (RNA-seq) and liquid chromatography-mass spectrometry (LC-MS), respectively. Upon *prx-5(RNAi)*, 1,372 genes and 120 proteins were significantly upregulated, whereas 662 genes and 57 proteins were significantly downregulated (Figures 6A and 6C; Table S2). We analyzed our RNA-seq and proteomics dataset for Gene Ontology (GO) enrichment using GOrilla (Eden et al., 2009) and REVIGO (REduce and VIsualize Gene Ontology) (Supek et al., 2011). This analysis revealed two large clusters of biological processes represented by the terms "immune response" and "lipid metabolic process" (Figures 6B and 6D; Table S3).

GO enrichment analysis also revealed that the GO terms "microbody" and "peroxisomes" were enriched in our RNA-seq and proteomics dataset (Table S3). To determine the fraction of peroxisomal proteins that had altered expression upon *prx-5(RNAi)*, we generated a list of 62 *C. elegans* peroxisomal proteins using literature searches, PeroxisomeDB (Schlüter et al., 2010) and WormBase (release WS272) (Lee et al., 2018; Table S4). Among the 53 peroxisomal proteins identified in our proteomics dataset, PRX-5 was the only significantly downregulated protein; 13 proteins were significantly upregulated, and the level of the remaining 39 proteins was not changed significantly upon *prx-5(RNAi)*. All upregulated proteins except one were peroxisomal matrix proteins. These proteins include the peroxisomal

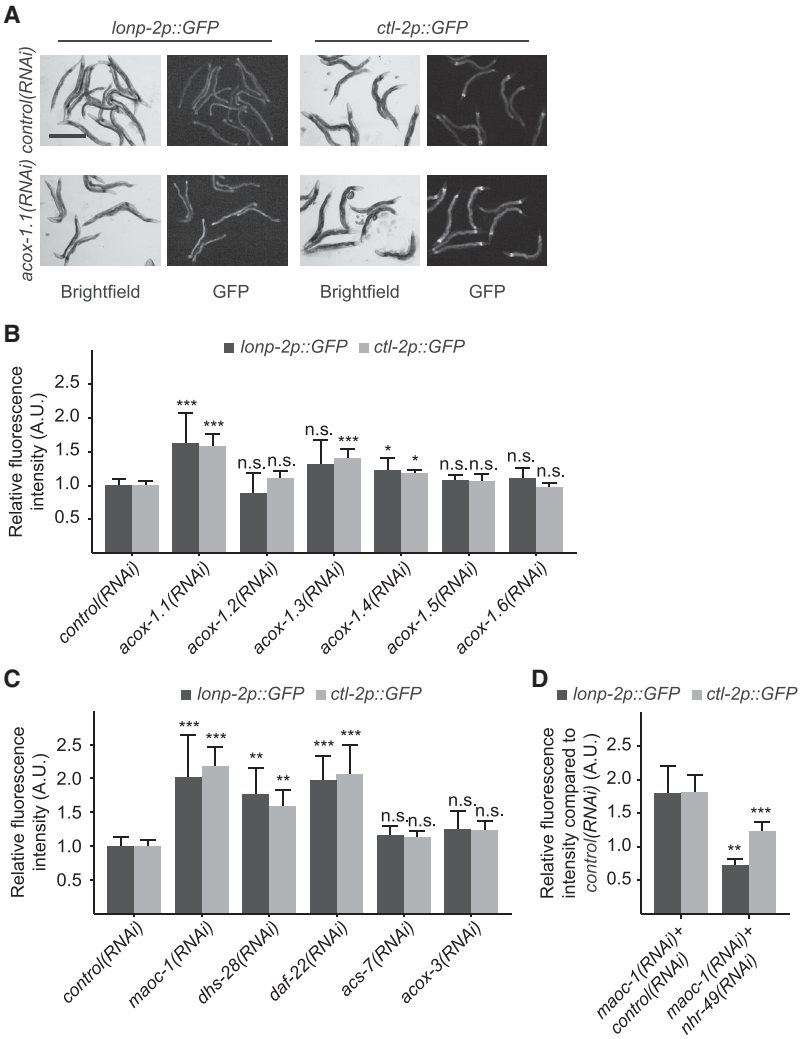

Figure 4. The PRS is activated by a defect in peroxisomal β-oxidation

(A) L4 larvae carrying the *lonp-2p::GFP* or *ctl-2p::GFP* reporter were subjected to different RNAi conditions. Adults of the next generation were analyzed by bright-field and fluorescence microscopy. Scale bar, 0.5 mm. Images were scaled with a minimum displayed value of 0 and a maximum displayed value that equals the maximum pixel value of the control. Although rescaling enhanced the signal, some pixels of the images are saturated. For details, see STAR methods. For unsaturated images, see Figure S3. Expression of the reporters was quantified relative to the *control(RNAi)*.

(B and C) Analysis of the effect of inactivation of acyl-CoA oxidases and other enzymes of peroxisomal β-oxidation on the PRS. n = 6–24 biological replicates; mean and SD are shown; *p < 0.05, **p < 0.01, and ***p < 0.001 by Kruskal-Wallis test with Dunn's multiple comparisons test to *control(RNAi)*.

(D) Analysis of the dependence on NHR-49 of *maoc-1(RNAi)*-induced activation of the PRS. The RNAi clones were diluted 1:2 with the RNAi clone indicated in the x axis label. n = 6 biological replicates; mean and SD are shown; **p < 0.01 and ***p < 0.001 by a (Welch) two-sample t test to *maoc-1(RNAi)* + *control(RNAi)*.

See also Figures S3 and S6.

catalase CTL-2, which is consistent with upregulation of *ctl-2p::GFP*. In contrast, we did not observe a significant change in the protein levels of the peroxisomal Lon protease. This result suggests that, in addition to transcriptional regulation, LONP-2 levels are also regulated at the post-transcriptional level. Finally, this analysis revealed that, among the 13 significantly upregulated peroxisomal proteins, 11 proteins are involved in peroxisomal β-oxidation. Using our list of 62 peroxisomal proteins, we analyzed our RNA-seq dataset (Table S4). Among the 57 corresponding genes identified in our RNA-seq dataset, 60% were upregulated significantly, and expression of the remaining genes was unchanged. Specifically, we found that genes encoding peroxisomal α- and β-oxidation enzymes as well as enzymes of the ether-phospholipid biosynthesis pathway were upregulated significantly. In addition, we found that almost all genes encoding peroxins, including *prx-5*, were upregulated significantly. We speculate that *prx-5* transcriptional upregulation is part of the PRS response and acts a compensatory mechanism in response to the decrease in peroxisomal protein import. Such an observation has already been made in the case of the UPR^{mt}, where the gene encoding the mitochondrial protease SPG-7 was upregulated in animals subjected to *spg-7(RNAi)* (Nargund et al., 2012). The discrepancy between our RNA-seq and our proteomics data with respect to *prx-5*/PRX-5 could be explained by the fact that animals for these two analyses were harvested in independent experiments but at the same time point (4 days after lay-off on RNAi plates). We speculate that, at this time, the transcriptional upregulation of *prx-5* observed by RNA-seq has not yet translated into an increase in PRX-5 protein level. These data show that genes/proteins involved in immune responses and peroxisomal lipid metabolism are targets of the PRS pathway and upregulated upon PRS activation.

Hallmarks of PRS activation are observed upon infection by *Pseudomonas aeruginosa*

GO enrichment analysis of the transcriptomics and proteomics data showed that genes/proteins belonging to the GO terms "immune response" and "innate immune response" are significantly enriched upon *prx-5(RNAi)*. Analysis of the RNA-seq data with the WormExp tool (Yang et al., 2016) revealed a significant overlap between genes upregulated upon PRS activation and genes upregulated during infection by pathogens such as *P. aeruginosa* PA14 or *Bacillus thuringiensis* BT247 (Nakad et al., 2016; Yang et al., 2015). In a consistent manner, there was a significant overlap between genes downregulated upon PRS activation and genes downregulated during infection (Nakad et al., 2016; Yang et al., 2015; Figure 7A). Class

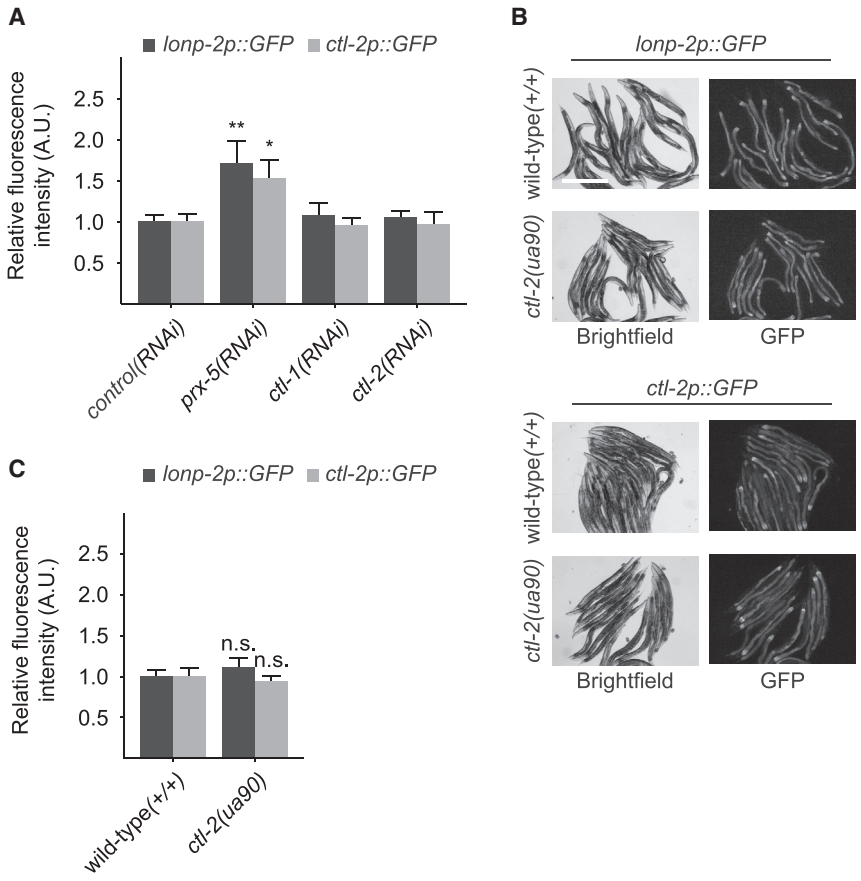

Figure 5. The PRS is not induced by a disruption of the redox balance between peroxisomes and the cytosol

(A) L4 larvae carrying the *lonp-2p::GFP* or *ctl-2p::GFP* reporter were subjected to different RNAi conditions. Adults of the next generation were analyzed by bright-field and fluorescence microscopy. Expression of the reporters was quantified relative to the *control(RNAi)*. n = 6 biological replicates; mean and SD are shown; *p < 0.05 and **p < 0.01 by Kruskal-Wallis test with Dunn's multiple comparisons test to *control(RNAi)*.

(B) Brightfield and fluorescence microscopy analysis of the *lonp-2p::GFP* or *ctl-2p::GFP* reporter carrying the *ctl-2(ua90)* mutation and the respective wild-type (+/+) strain. Scale bar, 0.5 mm. Images were scaled with a minimum displayed value of 0 and a maximum displayed value that equals the maximum pixel value of the control. Although rescaling enhanced the signal, some pixels of the images are saturated. For details, see STAR methods. For unsaturated images, see Figure S3.

(C) Quantification of the fluorescence intensity. n = 6 biological replicates; mean and SD are shown; n.s. by a two sample t test.

See also Figure S3.

enrichment analysis (Zugasti et al., 2016; J.J.E., unpublished data) showed similar results for the proteomics data. For instance, a significant overlap was identified between proteins upregulated upon PRS activation and genes upregulated upon *P. aeruginosa* infection and between proteins downregulated upon PRS activation and genes downregulated upon *P. aeruginosa* infection (Twumasi-Boateng and Shapira, 2012; Figure 7A). Similar to our observation, a subset of UPR^{mt} target genes has been shown to overlap with genes upregulated upon *P. aeruginosa* infection, and UPR^{mt} has been shown to be activated to mitigate mitochondrial damage upon *P. aeruginosa* infection (Pellegrino et al., 2014). We hypothesized that the PRS might likewise be activated upon infection with *P. aeruginosa*. To test this hypothesis, we exposed the PRS reporter strains (*lonp-2p::GFP*, *ctl-2p::GFP*, and *daf-22p::GFP*) to the *P. aeruginosa* strain PA14 for 4 h. Because *daf-22* is also upregulated upon PRS activation, we also generated and assayed a *daf-22p::GFP* transcriptional reporter. Exposure to the pathogen induced *ctl-2p::GFP* to almost the same extent as *prx-5(RNAi)* (1.6- versus 1.7-fold, respectively). *lonp-2p::GFP* and *daf-22p::GFP* expression increased 1.2- and 1.4-fold, respectively. Although the median of induction of *lonp-2p::GFP* expression was low, a proportion of animals showed strong induction (Figures 7B and 7C). These data are fully consistent with induction of the PRS upon exposure to a pathogen.

DISCUSSION

Our study revealed that peroxisomal import stress, caused by a 60% reduction in PRX-5 protein levels by RNAi, induces the transcriptional upregulation of the peroxisomal Lon protease and the peroxisomal catalase. We thus revealed the existence of a retrograde signaling mechanism from peroxisomes to the nucleus that we called the PRS. Lipidomics analysis revealed that *prx-5(RNAi)* animals exhibit increased levels of TGs with long acyl chains, indicating reduced β-oxidation activity. *prx-5(RNAi)* animals also have reduced levels of ether-PEs, which are generated exclusively in peroxisomes. These results indicate a general reduction of peroxisomal function, and in particular peroxisomal β-oxidation, in *prx-5(RNAi)* animals. Analysis of the proteome and transcriptome of *prx-5(RNAi)* animals revealed increased levels of peroxisomal β-oxidation enzymes. We speculate that upregulation of these enzymes upon *prx-5(RNAi)* might increase their probability to be recognized by the remaining PRX-5 receptors and to be imported into the remaining peroxisomes. We propose that activation of expression of these genes by the PRS is a mechanism to cope with reduced peroxisomal β-oxidation in response to peroxisomal import stress. We also observed, in our RNA-seq data, that the *prx-5* transcript was upregulated upon *prx-5(RNAi)*. As described above, we speculate that, at the time point where we performed our analyses, the upregulation of *prx-5* observed by RNA-seq did not yet translate into an increased PRX-5 protein level. This, however, means that, at a later time point, we could expect an increased level of PRX-5 protein, which could help with import of upregulated peroxisomal β-oxidation enzymes to restore peroxisomal function. We also observed, in our RNA-seq and proteomics data, upregulation of factors involved in immune

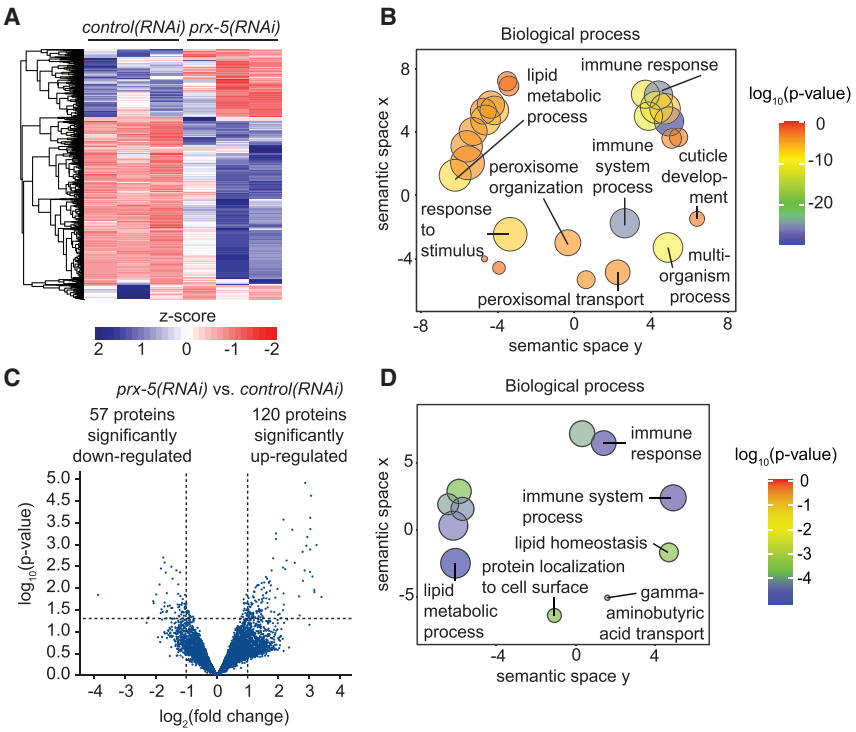

Figure 6. Transcriptomics and proteomics analyses of *C. elegans* animals treated with *prx-5(RNAi)*

(A) Wild-type L4 larvae were subjected to *prx-5(RNAi)*. Animals of the next generation were analyzed by RNA-seq and LC-MS. Shown is a heatmap comparing gene expression patterns of *prx-5(RNAi)* and *control(RNAi)* animals.

(B) GO enrichment analysis of genes significantly changed upon *prx-5(RNAi)*, summarized using REVIGO. Genes with a $\log_2$(fold change) ≥ 1 (increased) or ≤ -1 (decreased) and a false discovery rate (FDR) of less than 0.05 were considered significantly changed. GO terms are represented by circles and are plotted according to semantic similarities to other GO terms (adjoining circles are most closely related). The color indicates the $\log_{10}$(p).

(C) Volcano plot represents the $\log_2$(fold change) and $\log_{10}$(p) of identified proteins. Proteins with $p < 0.05$ and a $\log_2$(fold change) ≥ 1 (increased) or ≤ -1 (decreased) were considered significantly changed.

(D) GO enrichment analysis of proteins significantly changed upon *prx-5(RNAi)*, summarized using REVIGO.

See also Tables S2, S3, and S4.

responses upon PRS activation. Furthermore, we observed hallmarks of PRS activation upon infection with *P. aeruginosa*. *P. aeruginosa* toxins have been shown to interfere with mitochondrial function, and UPR^{mt} activation upon infection has been proposed as a mechanism to reduce mitochondrial damage caused by *P. aeruginosa* toxins (Pellegrino et al., 2014). Pec2, a recently identified virulence factor of *P. aeruginosa* important for *C. elegans* infection, has been shown to localize with microtubules, peroxisomes, and lipid droplets in infected cells. This suggests that Pec2 might affect transport of lipid droplets and/or peroxisomes and, hence, the ability of infected cells to metabolize lipids (Zrieq et al., 2015). We therefore speculate that the PRS has a second function and is part of a cellular surveillance mechanism against pathogen infection.

Our study also revealed that NHR-49, the functional homolog of PPARα, and its co-factor, the Mediator subunit MDT-15, act as transcription factors of the PRS. Feeding *C. elegans* with different fatty acids has been shown to change the expression of NHR-49 target genes (Xu et al., 2011). Furthermore, fatty acids have been shown to be natural ligands for PPARα (Kliewer et al., 1997). Thus, we speculate that fatty acids act as signaling molecules of the PRS. Consistent with this hypothesis, lipidomics analysis showed increased levels of TGs with longer acyl chains in *prx-5(RNAi)* animals. Furthermore, knockdown of genes encoding peroxisomal β-oxidation enzymes confirmed that blocking any step in the β-oxidation pathway can induce the PRS. We therefore speculate that a change in fatty acid composition activates NHR-49 and, thus, the PRS. We propose that specific fatty acids could be sensed by lipid binding proteins (LBPs), acyl-CoA binding proteins (ACBPs), or fatty acid/retinol binding proteins (FARs) and that these proteins would relay the signal to NHR-49. Consistent with this model, LBP-5 has been shown to be required for induction of transcription of NHR-49 target genes when *C. elegans* animals were raised in the presence of stearic acid (Xu et al., 2011). We observed that knockdown of only specific acyl-CoA oxidases induces the PRS. Different acyl-CoA oxidases have been shown to have different substrate specificity (Zhang et al., 2018). Thus, it is possible that only specific fatty acids act as signaling molecules. We also propose that, in case peroxisomal import and, thus, peroxisomal β-oxidation are restored, fatty acids that act as ligands of NHR-49 would be again processed normally, and the PRS would be turned off. As mentioned above, we speculate that the *P. aeruginosa* virulence factor Pec2 might affect the ability of infected cells to metabolize lipids. This could cause a change in fatty acid composition that could activate the PRS through NHR-49. Consistent with this idea, the PPARα agonist fenofibrate has been shown recently to increase *C. elegans* resistance to *P. aeruginosa* infection in a manner dependent on NHR-49 (Naim et al., 2020).

Other organelle retrograde signaling pathways (such as the mitochondrial or endoplasmic reticulum [ER] UPR) have been shown to be conserved from *C. elegans* to mammals. We speculate that the PRS might also be conserved in mammals. Consistent with this idea, the peroxisomal catalase has been shown to be transcriptionally upregulated in mouse neural cells deficient in *PEX5* (Bottelbergs et al., 2012). Furthermore, consistent with the PRS being activated by a defect in peroxisomal β-oxidation, mouse microglial cells lacking acyl-CoA oxidase 1 (*ACOX1*$^{-/-}$) also exhibit an increase in peroxisomal catalase activity (Raas et al., 2019).

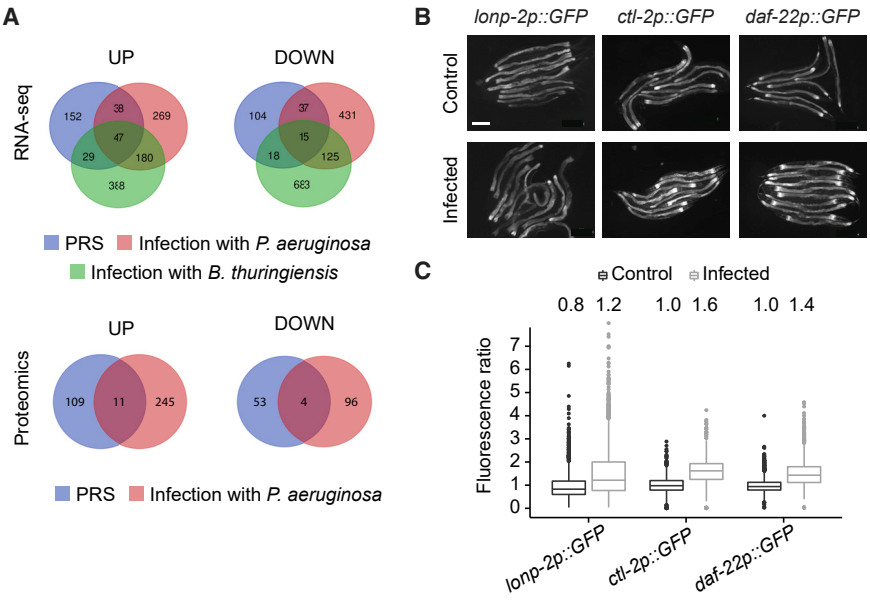

Figure 7. PRS genes are induced upon infection

(A) Venn diagram showing overlap between genes upregulated (or downregulated) in animals infected with *P. aeruginosa* or *B. thuringiensis* and genes upregulated (or downregulated) upon *prx-5(RNAi)* (PRS). A similar analysis was performed with the proteomics data.

(B) Young adults carrying the *lonp-2p::GFP*, *ctl-2p::GFP*, or *daf-22p::GFP* reporters were infected with *P. aeruginosa* (PA14) or left on *E. coli* (OP50) control plates. After 4 h of infection, the animals were analyzed by fluorescence microscopy. Scale bar, 200 μm. Images were scaled with a minimum displayed value of 0 and a maximum displayed value that equals the maximum pixel value of the control. Although rescaling enhanced the signal, some pixels of the images are saturated. For detail, see STAR methods. For unsaturated images, see Figure S3.

(C) Quantification of the relative fluorescence intensity of control (non-infected) animals or after 4 h of infection. The values show the median of the fold change. n = 457–1,407 animals.

See also Figure S3.

Finally, *ACOX1*$^{-/-}$ mice exhibit increased PPARα activity, suggesting that substrates of acyl-CoA oxidase might act as natural ligands for PPARα (Fan et al., 1998), similar to what we speculate for NHR-49. If the PRS is indeed conserved, then understanding its role in maintenance of peroxisomal function in mammals could contribute to our understanding of innate immunity and metabolic disorders.

STAR★METHODS

Detailed methods are provided in the online version of this paper and include the following:

- KEY RESOURCES TABLE
- RESOURCE AVAILABILITY
  - Lead contact
  - Materials availability
  - Data and code availability
- EXPERIMENTAL MODEL AND SUBJECT DETAILS
  - General *C. elegans* maintenance and strains
  - Transgenic animals
- METHOD DETAILS
  - RNA interference experiments
  - Protein quantification
  - RT-qPCR
  - RNA-seq analysis
  - Lipidomic analysis
  - Analysis of the effect of PA14 infection on the expression of the PRS reporters
  - Image analysis and image representation
- QUANTIFICATION AND STATISTICAL ANALYSIS

SUPPLEMENTAL INFORMATION

Supplemental Information can be found online at https://doi.org/10.1016/j.celrep.2020.108653.

ACKNOWLEDGMENTS

We thank B. Conradt, M. Fransen, E. Lambie, and N. Memar for comments on the manuscript. We also thank I. van der Klei and D. Leister for suggestions regarding the project. We also thank M. Gerstner for advice regarding statistical analysis of the data. We thank N. Lebedeva, M. Schwarz, and M. Bauer for excellent technical support and the Caenorhabditis Genetics Center (supported by the National Institutes of Health National Center for Research Resources) for strains. Work in S.G.R.'s lab was supported by the Deutsche Forschungsgemeinschaft (RO5352/1-1). S.G.R.'s work was also supported by the Institute for Basic Science (IBS-R022-A2-2020). E.R. is a member of the Life Science Munich graduate program. Work in A.I.'s lab is partly financed by a grant from the Deutsche Forschungsgemeinschaft (CRC1064/Z2). Work in J.J.E.'s lab is supported by institutional grants from INSERM, CNRS, and AMU and an Agence Nationale de la Recherche program grant (ANR-16-CE15-0001-01). Z.X. is a recipient of a fellowship from the Chinese Scholarship Council. Work in M.W.'s lab was supported by the Deutsche Forschungsgemeinschaft (WI4382/11-1). C.O. and S.S. are supported by a grant from the European Research Council (ERCStG-714739 IlluMitoDNA).

AUTHOR CONTRIBUTIONS

E.R and S.G.R. designed and conducted the experiments and wrote the paper. I.F. and A.I. designed and conducted the proteomics experiments and contributed to writing of the proteomics part of the paper. X.Z. and J.J.E. designed and conducted the infection experiments and contributed to writing of the infection part of the paper. J.J.E. and C.O. contributed to writing of the paper. M.W. designed and conducted the lipidomics experiments and contributed to writing of the lipidomics part of the paper. J.Z. prepared the worm samples for the RNA-seq and lipidomics experiments. S.S. and C.O. designed and conducted the qRT-PCR experiments and contributed to writing of the RT-qPCR part of the paper. C.F. generated the Fiji Macro and contributed to writing of the image analysis part of the paper.

DECLARATION OF INTERESTS

The authors declare no competing interests.

Received: September 24, 2019
Revised: October 6, 2020
Accepted: December 22, 2020
Published: January 19, 2021

REFERENCES

Aksam, E.B., Koek, A., Kiel, J.A., Jourdan, S., Veenhuis, M., and van der Klei, I.J. (2007). A peroxisomal lon protease and peroxisome degradation by autophagy play key roles in vitality of *Hansenula polymorpha* cells. Autophagy *3*, 96–105.

Artyukhin, A.B., Zhang, Y.K., Akagi, A.E., Panda, O., Sternberg, P.W., and Schroeder, F.C. (2018). Metabolomic "Dark Matter" Dependent on Peroxisomal β-Oxidation in *Caenorhabditis elegans*. J. Am. Chem. Soc. *140*, 2841–2852.

Bartoszewska, M., Williams, C., Kikhney, A., Opaliński, Ł., van Roermund, C.W., de Boer, R., Veenhuis, M., and van der Klei, I.J. (2012). Peroxisomal proteostasis involves a Lon family protein that functions as protease and chaperone. J. Biol. Chem. *287*, 27380–27395.

Botman, D., de Groot, D.H., Schmidt, P., Goedhart, J., and Teusink, B. (2019). *In vivo* characterisation of fluorescent proteins in budding yeast. Sci. Rep. *9*, 2234.

Bottelbergs, A., Verheijden, S., Van Veldhoven, P.P., Just, W., Devos, R., and Baes, M. (2012). Peroxisome deficiency but not the defect in ether lipid synthesis causes activation of the innate immune system and axonal loss in the central nervous system. J. Neuroinflammation *9*, 61.

Brenner, S. (1974). The genetics of *Caenorhabditis elegans*. Genetics *77*, 71–94.

Butcher, R.A., Fujita, M., Schroeder, F.C., and Clardy, J. (2007). Small-molecule pheromones that control dauer development in *Caenorhabditis elegans*. Nat. Chem. Biol. *3*, 420–422.

Butcher, R.A., Ragains, J.R., Li, W., Ruvkun, G., Clardy, J., and Mak, H.Y. (2009). Biosynthesis of the *Caenorhabditis elegans* dauer pheromone. Proc. Natl. Acad. Sci. USA *106*, 1875–1879.

Drechsler, R., Chen, S.W., Dancy, B.C., Mehrabkhani, L., and Olsen, C.P. (2016). HPLC-Based Mass Spectrometry Characterizes the Phospholipid Alterations in Ether-Linked Lipid Deficiency Models Following Oxidative Stress. PLoS ONE *11*, e0167229.

Eden, E., Navon, R., Steinfeld, I., Lipson, D., and Yakhini, Z. (2009). GOrilla: a tool for discovery and visualization of enriched GO terms in ranked gene lists. BMC Bioinformatics *10*, 48.

Edgar, R., Domrachev, M., and Lash, A.E. (2002). Gene Expression Omnibus: NCBI gene expression and hybridization array data repository. Nucleic Acids Res. *30*, 207–210.

Fan, C.-Y., Pan, J., Usuda, N., Yeldandi, A.V., Rao, M.S., and Reddy, J.K. (1998). Steatohepatitis, spontaneous peroxisome proliferation and liver tumors in mice lacking peroxisomal fatty acyl-CoA oxidase. Implications for peroxisome proliferator-activated receptor α natural ligand metabolism. J. Biol. Chem. *273*, 15639–15645.

Francisco, T., Rodrigues, T.A., Dias, A.F., Barros-Barbosa, A., Bicho, D., and Azevedo, J.E. (2017). Protein transport into peroxisomes: Knowns and unknowns. BioEssays *39*, 1700047.

Frøkjær-Jensen, C., Davis, M.W., Ailion, M., and Jorgensen, E.M. (2012). Improved Mos1-mediated transgenesis in *C. elegans*. Nat. Methods *9*, 117–118.

Frøkjær-Jensen, C., Davis, M.W., Sarov, M., Taylor, J., Flibotte, S., LaBella, M., Pozniakovsky, A., Moerman, D.G., and Jorgensen, E.M. (2014). Random and targeted transgene insertion in *Caenorhabditis elegans* using a modified Mos1 transposon. Nat. Methods *11*, 529–534.

Golden, J.W., and Riddle, D.L. (1982). A pheromone influences larval development in the nematode *Caenorhabditis elegans*. Science *218*, 578–580.

Gurvitz, A., Langer, S., Piskacek, M., Hamilton, B., Ruis, H., and Hartig, A. (2000). Predicting the function and subcellular location of *Caenorhabditis elegans* proteins similar to *Saccharomyces cerevisiae* beta-oxidation enzymes. Yeast *17*, 188–200.

Hoogewijs, D., Houthoofd, K., Matthijssens, F., Vandesompele, J., and Vanfleteren, J.R. (2008). Selection and validation of a set of reliable reference genes for quantitative sod gene expression analysis in *C. elegans*. BMC Mol. Biol. *9*, 9.

Kamath, R.S., and Ahringer, J. (2003). Genome-wide RNAi screening in *Caenorhabditis elegans*. Methods *30*, 313–321.

Kind, T., Liu, K.H., Lee, D.Y., DeFelice, B., Meissen, J.K., and Fiehn, O. (2013). LipidBlast *in silico* tandem mass spectrometry database for lipid identification. Nat. Methods *10*, 755–758.

Kind, T., Okazaki, Y., Saito, K., and Fiehn, O. (2014). LipidBlast templates as flexible tools for creating new in-silico tandem mass spectral libraries. Anal. Chem. *86*, 11024–11027.

Kliewer, S.A., Sundseth, S.S., Jones, S.A., Brown, P.J., Wisely, G.B., Koble, C.S., Devchand, P., Wahli, W., Willson, T.M., Lenhard, J.M., and Lehmann, J.M. (1997). Fatty acids and eicosanoids regulate gene expression through direct interactions with peroxisome proliferator-activated receptors α and γ. Proc. Natl. Acad. Sci. USA *94*, 4318–4323.

Langmead, B., Trapnell, C., Pop, M., and Salzberg, S.L. (2009). Ultrafast and memory-efficient alignment of short DNA sequences to the human genome. Genome Biol. *10*, R25.

Lee, R.Y.N., Howe, K.L., Harris, T.W., Arnaboldi, V., Cain, S., Chan, J., Chen, W.J., Davis, P., Gao, S., Grove, C., et al. (2018). WormBase 2017: molting into a new stage. Nucleic Acids Res. *46* (*D1*), D869–D874.

Livak, K.J., and Schmittgen, T.D. (2001). Analysis of relative gene expression data using real-time quantitative PCR and the 2(-Δ Δ C(T)) Method. Methods *25*, 402–408.

Löfgren, L., Ståhlman, M., Forsberg, G.B., Saarinen, S., Nilsson, R., and Hansson, G.I. (2012). The BUME method: a novel automated chloroform-free 96-well total lipid extraction method for blood plasma. J. Lipid Res. *53*, 1690–1700.

Mello, C.C., Kramer, J.M., Stinchcomb, D., and Ambros, V. (1991). Efficient gene transfer in *C.elegans*: extrachromosomal maintenance and integration of transforming sequences. EMBO J. *10*, 3959–3970.

Motley, A.M., Hettema, E.H., Ketting, R., Plasterk, R., and Tabak, H.F. (2000). *Caenorhabditis elegans* has a single pathway to target matrix proteins to peroxisomes. EMBO Rep. *1*, 40–46.

Naim, N., Amrit, F.R., Ratnappan, R., DelBuono, N., Loose, J.A., and Ghazi, A. (2020). NHR-49 Acts in Distinct Tissues to Promote Longevity versus Innate Immunity. bioRxiv. https://doi.org/10.1101/2020.2009.2011.290452.

Nakad, R., Snoek, L.B., Yang, W., Ellendt, S., Schneider, F., Mohr, T.G., Rösingh, L., Masche, A.C., Rosenstiel, P.C., Dierking, K., et al. (2016). Contrasting invertebrate immune defense behaviors caused by a single gene, the *Caenorhabditis elegans* neuropeptide receptor gene npr-1. BMC Genomics *17*, 280.

Nargund, A.M., Pellegrino, M.W., Fiorese, C.J., Baker, B.M., and Haynes, C.M. (2012). Mitochondrial import efficiency of ATFS-1 regulates mitochondrial UPR activation. Science *337*, 587–590.

Pathare, P.P., Lin, A., Bornfeldt, K.E., Taubert, S., and Van Gilst, M.R. (2012). Coordinate regulation of lipid metabolism by novel nuclear receptor partnerships. PLoS Genet. *8*, e1002645.

Pellegrino, M.W., Nargund, A.M., and Haynes, C.M. (2013). Signaling the mitochondrial unfolded protein response. Biochim. Biophys. Acta *1833*, 410–416.

Pellegrino, M.W., Nargund, A.M., Kirienko, N.V., Gillis, R., Fiorese, C.J., and Haynes, C.M. (2014). Mitochondrial UPR-regulated innate immunity provides resistance to pathogen infection. Nature *516*, 414–417.

Perez-Riverol, Y., Csordas, A., Bai, J., Bernal-Llinares, M., Hewapathirana, S., Kundu, D.J., Inuganti, A., Griss, J., Mayer, G., Eisenacher, M., et al. (2019). The PRIDE database and related tools and resources in 2019: improving support for quantification data. Nucleic Acids Res. *47* (*D1*), D442–D450.

Petriv, O.I., and Rachubinski, R.A. (2004). Lack of peroxisomal catalase causes a progeric phenotype in *Caenorhabditis elegans*. J. Biol. Chem. *279*, 19996–20001.

Petriv, O.I., Pilgrim, D.B., Rachubinski, R.A., and Titorenko, V.I. (2002). RNA interference of peroxisome-related genes in *C. elegans*: a new model for human peroxisomal disorders. Physiol. Genomics *10*, 79–91.

Pinto, M.P., Grou, C.P., Alencastre, I.S., Oliveira, M.E., Sá-Miranda, C., Fransen, M., and Azevedo, J.E. (2006). The import competence of a peroxisomal membrane protein is determined by Pex19p before the docking step. J. Biol. Chem. *281*, 34492–34502.

Powell, J.R., and Ausubel, F.M. (2008). Models of *Caenorhabditis elegans* infection by bacterial and fungal pathogens. Methods Mol. Biol. *415*, 403–427.

Pujol, N., Cypowyj, S., Ziegler, K., Millet, A., Astrain, A., Goncharov, A., Jin, Y., Chisholm, A.D., and Ewbank, J.J. (2008). Distinct innate immune responses to infection and wounding in the *C. elegans* epidermis. Curr. Biol. *18*, 481–489.

R Core Team (2017). R: A Language and Environment for Statistical Computing (R Foundation for Statistical Computing).

Raas, Q., Saih, F.E., Gondcaille, C., Trompier, D., Hamon, Y., Leoni, V., Caccia, C., Nasser, B., Jadot, M., Ménétrier, F., et al. (2019). A microglial cell model for acyl-CoA oxidase 1 deficiency. Biochim. Biophys. Acta Mol. Cell Biol. Lipids *1864*, 567–576.

Rahme, L.G., Stevens, E.J., Wolfort, S.F., Shao, J., Tompkins, R.G., and Ausubel, F.M. (1995). Common virulence factors for bacterial pathogenicity in plants and animals. Science *268*, 1899–1902.

Rolland, S.G., Schneid, S., Schwarz, M., Rackles, E., Fischer, C., Haeussler, S., Regmi, S.G., Yeroslaviz, A., Habermann, B., Mokranjac, D., et al. (2019). Compromised Mitochondrial Protein Import Acts as a Signal for UPRmt. Cell Rep. *28*, 1659–1669.e5.

Rual, J.-F., Ceron, J., Koreth, J., Hao, T., Nicot, A.-S., Hirozane-Kishikawa, T., Vandenhaute, J., Orkin, S.H., Hill, D.E., van den Heuvel, S., and Vidal, M. (2004). Toward improving *Caenorhabditis elegans* phenome mapping with an ORFeome-based RNAi library. Genome Res. *14* (*10B*), 2162–2168.

Rueden, C.T., Schindelin, J., Hiner, M.C., DeZonia, B.E., Walter, A.E., Arena, E.T., and Eliceiri, K.W. (2017). ImageJ2: ImageJ for the next generation of scientific image data. BMC Bioinformatics *18*, 529.

Sasaki, K., and Yoshida, H. (2015). Organelle autoregulation-stress responses in the ER, Golgi, mitochondria and lysosome. J. Biochem. *157*, 185–195.

Schindelin, J., Arganda-Carreras, I., Frise, E., Kaynig, V., Longair, M., Pietzsch, T., Preibisch, S., Rueden, C., Saalfeld, S., Schmid, B., et al. (2012). Fiji: an open-source platform for biological-image analysis. Nat. Methods *9*, 676–682.

Schlüter, A., Real-Chicharro, A., Gabaldón, T., Sánchez-Jiménez, F., and Pujol, A. (2010). PeroxisomeDB 2.0: an integrative view of the global peroxisomal metabolome. Nucleic Acids Res. *38*, D800–D805.

Shi, X., Tarazona, P., Brock, T.J., Browse, J., Feussner, I., and Watts, J.L. (2016). A *Caenorhabditis elegans* model for ether lipid biosynthesis and function. J. Lipid Res. *57*, 265–275.

Srinivasan, J., Kaplan, F., Ajredini, R., Zachariah, C., Alborn, H.T., Teal, P.E.A., Malik, R.U., Edison, A.S., Sternberg, P.W., and Schroeder, F.C. (2008). A blend of small molecules regulates both mating and development in *Caenorhabditis elegans*. Nature *454*, 1115–1118.

Srinivasan, J., von Reuss, S.H., Bose, N., Zaslaver, A., Mahanti, P., Ho, M.C., O'Doherty, O.G., Edison, A.S., Sternberg, P.W., and Schroeder, F.C. (2012). A modular library of small molecule signals regulates social behaviors in *Caenorhabditis elegans*. PLoS Biol. *10*, e1001237.

Stiernagle, T. (2006). Maintenance of C. elegans.http://www.wormbook.org/chapters/www_strainmaintain/strainmaintain.html.

Supek, F., Bošnjak, M., Škunca, N., and Šmuc, T. (2011). REVIGO summarizes and visualizes long lists of gene ontology terms. PLoS ONE *6*, e21800.

Taubert, S., Van Gilst, M.R., Hansen, M., and Yamamoto, K.R. (2006). A Mediator subunit, MDT-15, integrates regulation of fatty acid metabolism by NHR-49-dependent and -independent pathways in *C. elegans*. Genes Dev. *20*, 1137–1149.

Thieringer, H., Moellers, B., Dodt, G., Kunau, W.-H., and Driscoll, M. (2003). Modeling human peroxisome biogenesis disorders in the nematode *Caenorhabditis elegans*. J. Cell Sci. *116*, 1797–1804.

Twumasi-Boateng, K., and Shapira, M. (2012). Dissociation of immune responses from pathogen colonization supports pattern recognition in *C. elegans*. PLoS ONE *7*, e35400.

Van Gilst, M.R., Hadjivassiliou, H., Jolly, A., and Yamamoto, K.R. (2005). Nuclear hormone receptor NHR-49 controls fat consumption and fatty acid composition in *C. elegans*. PLoS Biol. *3*, e53.

Van Veldhoven, P.P. (2010). Biochemistry and genetics of inherited disorders of peroxisomal fatty acid metabolism. J. Lipid Res. *51*, 2863–2895.

Viswakarma, N., Jia, Y., Bai, L., Vluggens, A., Borensztajn, J., Xu, J., and Reddy, J.K. (2010). Coactivators in PPAR-Regulated Gene Expression. PPAR Res. *2010*, 21.

von Reuss, S.H., Bose, N., Srinivasan, J., Yim, J.J., Judkins, J.C., Sternberg, P.W., and Schroeder, F.C. (2012). Comparative metabolomics reveals biogenesis of ascarosides, a modular library of small-molecule signals in *C. elegans*. J. Am. Chem. Soc. *134*, 1817–1824.

Wiemer, E.A., Nuttley, W.M., Bertolaet, B.L., Li, X., Francke, U., Wheelock, M.J., Anné, U.K., Johnson, K.R., and Subramani, S. (1995). Human peroxisomal targeting signal-1 receptor restores peroxisomal protein import in cells from patients with fatal peroxisomal disorders. J. Cell Biol. *130*, 51–65.

Xu, M., Joo, H.-J., and Paik, Y.-K. (2011). Novel functions of lipid-binding protein 5 in *Caenorhabditis elegans* fat metabolism. J. Biol. Chem. *286*, 28111–28118.

Yang, W., Dierking, K., Esser, D., Tholey, A., Leippe, M., Rosenstiel, P., and Schulenburg, H. (2015). Overlapping and unique signatures in the proteomic and transcriptomic responses of the nematode *Caenorhabditis elegans* toward pathogenic *Bacillus thuringiensis*. Dev. Comp. Immunol. *51*, 1–9.

Yang, W., Dierking, K., and Schulenburg, H. (2016). WormExp: a web-based application for a *Caenorhabditis elegans*-specific gene expression enrichment analysis. Bioinformatics *32*, 943–945.

Yoneda, T., Benedetti, C., Urano, F., Clark, S.G., Harding, H.P., and Ron, D. (2004). Compartment-specific perturbation of protein handling activates genes encoding mitochondrial chaperones. J. Cell Sci. *117*, 4055–4066.

Zhang, S.O., Box, A.C., Xu, N., Le Men, J., Yu, J., Guo, F., Trimble, R., and Mak, H.Y. (2010). Genetic and dietary regulation of lipid droplet expansion in *Caenorhabditis elegans*. Proc. Natl. Acad. Sci. USA *107*, 4640–4645.

Zhang, X., Wang, Y., Perez, D.H., Jones Lipinski, R.A., and Butcher, R.A. (2018). Acyl-CoA Oxidases Fine-Tune the Production of Ascaroside Pheromones with Specific Side Chain Lengths. ACS Chem. Biol. *13*, 1048–1056.

Zhou, Y., Wang, Y., Zhang, X., Bhar, S., Jones Lipinski, R.A., Han, J., Feng, L., and Butcher, R.A. (2018). Biosynthetic tailoring of existing ascaroside pheromones alters their biological function in *C. elegans*. eLife *7*, e33286.

Zrieq, R., Sana, T.G., Vergin, S., Garvis, S., Volfson, I., Bleves, S., Voulhoux, R., and Hegemann, J.H. (2015). Genome-wide Screen of *Pseudomonas aeruginosa* in *Saccharomyces cerevisiae* Identifies New Virulence Factors. Front. Cell. Infect. Microbiol. *5*, 81.

Zugasti, O., Thakur, N., Belougne, J., Squiban, B., Kurz, C.L., Soulé, J., Omi, S., Tichit, L., Pujol, N., and Ewbank, J.J. (2016). A quantitative genome-wide RNAi screen in *C. elegans* for antifungal innate immunity genes. BMC Biol. *14*, 35.

STAR★METHODS

KEY RESOURCES TABLE

REAGENT or RESOURCE	SOURCE	IDENTIFIER
Bacterial and virus strains		
RNAi clones Ahringer library	Kamath and Ahringer, 2003	N/A
RNAi clones Vidal library	Rual et al., 2004	N/A
OP50	Caenorhabditis Genetics Center	OP50
HT115	Caenorhabditis Genetics Center	HT115
DH5α	ThermoFischer	Cat # 18265017
Pseudomonas aeruginosa PA14	Rahme et al., 1995	PA14
Chemicals, reptides, and recombinant proteins		
IPTG	Carl-Roth	Cat # CN08.2
iTaq Universal SYBR Green Supermix	Bio-Rad	Cat # 1725120
Critical commercial assays		
ProtoScript® II First Strand cDNA Synthesis Kit	New England BioLabs	Cat # E6560S
RNeasy Mini Kit	QIAGEN	Cat # 74104
iST 8x Kit	PreOmics GmbH	https://www.preomics.com/
25cm Aurora Series emitter column (25cm x 75μm ID, 1.6μm C18)	Ionopticks	https://www.ionopticks.com/
Deposited data		
Mass spectrometry proteomics data	This study	PRIDE: PXD014720
RNA-seq data	This study	GEO: GSE156318
Experimental models: organisms/strains		
Wildtype C. elegans strain N2	Caenorhabditis Genetics Center	N2
SJ4100 (*zcIs13* V)	Caenorhabditis Genetics Center	SJ4100
LB90 (*ctl-2(ua90) II*)	Caenorhabditis Genetics Center	LB90
MD3919 (*bcIs126*)	This study	N/A
MD4253 (*bcSi76 IV*)	This study	N/A
MD4381 (*bcIs126; ctl-2(ua90) II*)	This study	N/A
MD4665 (*ctl-2(ua90) II; bcSi76 IV*)	This study	N/A
MD4664 (*bcSi76 IV*)	This study	N/A
MD4667 (*bcSi118 IV*: *bcSi119 X*)	This study	N/A
MD4581 (*bcSi110*)	This study	N/A
MD4272 (*bcIs140; lin-15*(*n765*ts))	This study	N/A
Oligonucleotides		
Primers for cloning (Table S5)	This study	N/A
Primers for RT-qPCR (Table S5)	This study	N/A
Recombinant DNA		
pCFJ350 (empty MosSCI vector)	Addgene	Plasmid #34866
pPD95_75 (empty backbone)	Addgene	Plasmid #1494
pCFJ909 (empty MiniMos vector)	Addgene	Plasmid # 44480
pPD118.60 (empty backbone)	Addgene	Plasmid #1598
pPD129.36 (empty backbone)	Addgene	Plasmid # 1654
pBluescript KS(+) (empty backbone)	Stratagene	N/A
pBC1503 (*lonp-2p::GFP*)	This study	N/A

(*Continued on next page*)

Continued

REAGENT or RESOURCE	SOURCE	IDENTIFIER
pBC1744 (ctl-2p::GFP)	This study	N/A
pBC1699 (*vha-7p::mKate2::linker::pxmp-4*)	This study	N/A
pBC1578 (*vha-7p::GFP::PTS1*)	This study	N/A
pBC1918 (*daf-22p::mKate2::linker::daf-22*)	This study	N/A
pBC1945 (*daf-22p::GFP::linker::pxmp-4*)	This study	N/A
pBC1905 (*daf-22p::GFP)*	This study	N/A
Software and algorithms		
Leica Application Suite (3.2.0.9652)	Leica Microsystems	https://www.leica-microsystems.com/products/microscope-software/p/leica-application-suite/
MetaMorph software (7.1.0.0)	Molecular Devices	https://www.moleculardevices.com/
R (3.6.1)	R Core Team, 2017	https://www.r-project.org/
Fiji/ImageJ2 (1.52p)	Rueden et al., 2017; Schindelin et al., 2012	https://imagej.net/Welcome
MaxQuant (1.5.2.8)	Freeware	https://www.maxquant.org
Genedata Expressionist for Mass Spectrometry (13.5)	Genedata	https://www.genedata.com/

RESOURCE AVAILABILITY

Lead contact

Further information and requests for resources and reagents should be directed to and will be fulfilled by the Lead Contact, Stéphane G. Rolland (srolland@ibs.re.kr).

Materials availability

All *C. elegans* strains and plasmids generated in this study are freely available upon request to the Lead Contact, Stéphane G. Rolland (srolland@ibs.re.kr).

Data and code availability

The mass spectrometry proteomics data have been deposited to the ProteomeXchange Consortium via the PRIDE (Perez-Riverol et al., 2019) partner repository (PRIDE: PXD014720). The RNA-seq data has been deposited in NCBI's Gene Expression Omnibus (Edgar et al., 2002) (GEO : GSE156318). The lipidomic data is included in Table S1. The Fiji script for image analysis is included in the Data S1 file.

EXPERIMENTAL MODEL AND SUBJECT DETAILS

General *C. elegans* maintenance and strains

C. elegans strains were cultured as previously described (Brenner, 1974). Bristol N2 was used as the wild-type strain. The following alleles and transgenes were used: *zcIs13* (*hsp-6p::GFP*) (Yoneda et al., 2004), *bcIs126 (lonp-2p::GFP)* (this study), *bcSi76 (ctl-2p::GFP)* IV (this study), *bcSi118;bcSi119 (daf-22p::mKate2::daf-22* and *daf-22p::GFP::pxmp-4)* (this study), *bcIs140;lin-15(n765*ts*)* (*vha-7p::mKate2::pxmp-4* and *vha-7p::GFP::PTS1*) (this study), *bcSi110* (*daf-22p::GFP*) (this study), *bcIs126;ctl-2(ua90)* II (this study) and *bcSi76* IV*;ctl-2(ua90)* II (this study). For the killing assay, we used the *Pseudomonas aeruginosa* PA14 strain (Rahme et al., 1995).

Transgenic animals

To construct the *lonp-2p::GFP* transcriptional reporter, a 1kb fragment immediately 5′ of the predicted start codon of *lonp-2* was amplified from *C. elegans* genomic DNA using the primers 5′-GCATGCTTGAGCAGAAAAATTGAGGC-3′ and 5′-GGTACCT TCATTTCGGGCAAAACTG-3′. The fragment was ligated into the SphI and KpnI sites of pBluescript KS(+) (Stratagene) generating the plasmid pBC1502. The promoter was sub-cloned in front of *GFP* in the plasmid pPD95_75 (a gift from Andrew Fire; Addgene plasmid no. 1494) to generate the plasmid pBC1503. The transgenic line containing the multi-copy extrachromosomal array (*bcEx1228*) was generated by co-injection of the plasmid pBC1503 (5 ng/μl) with pRF4 (80 ng/μl), which contains the *rol-6(su1006 dm)* allele (Mello et al., 1991). The extrachromosomal array was then integrated by UV treatment to generate the *lonp-2p::GFP* reporter strain *(bcIs126)* and was backcrossed five times with N2.

The *ctl-2p::GFP* transcriptional reporter was generated by amplifying a 1.6 kb fragment immediately 5′ of the predicted start codon of *ctl-2* from *C. elegans* genomic DNA using the primers 5′-GCATGCACTTTTGTATATAGAATCTCG-3′ and 5′-ACCG GTTTTGGTTCTGAAATTTTAGTTAGG-3′. BLAST analysis showed that the promoter of *ctl-1* and *ctl-2* are identical and, therefore, the reporter also shows the transcriptional regulation of *ctl-1*. To generate the plasmid pBC1690, the *lonp-2* promoter of the plasmid pBC1503 was replaced by the *ctl-2* promoter using the SphI and AgeI restriction sites. The *ctl-2p::GFP* fusion construct was then amplified from the plasmid pBC1690 with the primers 5′-ACGTCACCGGTTCTAGATACACTTTTGTATATAGAATCTCGTTATTT ATAAAC-3′ and 5′-TAGAGGGTACCAGAGCTCACAAACAGTTATGG-3′. The PCR product was ligated by Gibson cloning into the AvrII site of the MosSCI vector pCFJ350 (a gift from Erik Jorgensen; Addgene plasmid no. 34866) (Frøkjær-Jensen et al., 2012), which contains the *cb-unc-119(+)* rescue fragment. The final plasmid was named pBC1744. The single-copy insertion *bcSi76* on LGIV was generated by microinjection of the plasmid pBC1744 into the strain EG8081 [*oxTi177; unc-119(ed3)*] using MosSCI (Frøkjær-Jensen et al., 2012).

The *daf-22p::GFP* reporter was generated by amplifying a 2.3 kb fragment immediately 5′ of the predicted start codon of *daf-22* from *C. elegans* genomic DNA using the primers 5′-AAGCTACGTAATACGACTCAATGGCTTTACCACCAATTG-3′ and 5′-CTTTAC TCATTTTTCTGGAACAATATTTTTTTTTC-3′. The *GFP::unc-54 3′UTR* fusion construct was amplified from the plasmid pBC1744 using the primers 5′-TTCCAGAAAAATGAGTAAAGGAGAAGAAC-3′ and 5′-TTCGAAGATCTGCCCACTAGAAACAGTTATGTTTG GTATATTG-3′. The two PCR products were inserted by Gibson assembly into the SpeI site of the MiniMos vector pCFJ909 (a gift from Erik Jorgensen; Addgene plasmid no. 44480), which harbors the *cb-unc-119(+)* rescue fragment. Microinjection of the obtained plasmid pBC1905 (10 ng/μl) into the strain HT1593 [*unc-119(ed3)*] using MiniMos (Frøkjær-Jensen et al., 2014) generated the single-copy insertion allele *bcSi110*.

To label the peroxisomal membrane in epidermal cells, a fusion construct of mKate2 with the peroxisomal membrane protein PXMP-4 was generated. *mKate2* was amplified by PCR using the primers 5′-GCTAGCATGTCCGAGCTCATCAAGGAG-3′ and 5′-GGGAGCGCAGGCCGGAACGGTGTCCGAGCTTG-3′. *pxmp-4* fused to a 5′ linker (The 5′ linker codes for the following amino-acid sequence: SGLRSRAQASNS.) was amplified using the primers 5′-CAAGCTCGGACACCGTTCCGGCCTGCGCTCCC-3′ and 5′-GGTACCCTATGGATGGAATTCGAATAGCC −3′. The two PCR products were fused by overlap extension PCR using the primers 5′- GCTAGCATGTCCGAGCTCATCAAGGAG −3′ and 5′-GGTACCCTATGGATGGAATTCGAATAGCC-3′. To generate the plasmid pBC1691, the obtained PCR product was cloned into the EcoRV site of pBluescript KS(+) (Stratagene) . The *mKate2::linker::pxmp-4* fusion construct was sub-cloned into the NheI KpnI sites of pBC1666, which contained the *vha-7* promoter and an *unc-54* 3′UTR to generate the plasmid pBC1699. To label the peroxisomal matrix in epidermal cells, a *GFP::PTS1* construct was generated. *GFP* was amplified from the plasmid pPD118.60 (a gift from Andrew Fire; Addgene plasmid no. 1598) using the primers 5′-GGTACCATGAGTAAAGGAGAAGAACTTTTC-3′ and 5′-GAATTCTTAAAGTTTGGAATGAAGAGGTTTG-3′. The PCR product was cloned into the EcoRV site of pBluescript KS(+) (Stratagene) to generate the plasmid pBC1572. The *GFP::PTS1* was sub-cloned into the KpnI SacI sites of the plasmid pBC970, which contained the *vha-7* promoter and an *unc-54* 3′ UTR. The obtained plasmid was named pBC1578. To generate a reporter expressing mKate2 labeled peroxisomal membrane and GFP labeled peroxisomal matrix, the plasmids pBC1699 (1 ng/μl) and pBC1578 (1 ng/μl) were co-injected into MT4162 (*lin-15(n765ts)*). The *lin-15* rescue plasmid pL15.EK (50 ng/μl) was used as a co-injection marker. The extrachromosomal array was then integrated by UV treatment and the obtained *vha-7p::GFP::PTS1 and vha-7p::mKate2::pxmp-4 (bcIs140; lin-15*(*n765*ts)) reporter strain was backcrossed five times with N2.

To label peroxisomes by a *mKate2::daf-22* fusion protein, 2.3 kb of the *daf-22* promoter was amplified from the plasmid pBC1905 using the primers 5′-AAGCTACGTAATACGACTCAATGGCTTTACCACCAATTG-3′ and 5′GAGCTCGGACATTTTTCTGGAA CAATATTTTTTTTTCGAAG-3′. The *daf-22* coding sequence and its 3′ UTR was amplified from *C. elegans* genomic DNA using the primers 5′-GCGTCCAACTCCATGACGCCAACCAAGCCAAAG-3′ and 5′-CGCGATGCATTCGAAGATCTGCCCAAGTTAGTTTT TTACTAGAAGCTGCC-3′. mKate2 fused to a linker was amplified from the plasmid pBC1699 using the primers 5′-TTGTTCC AGAAAAATGTCCGAGCTCATCAAGGAG-3′ and 5′TGGTTGGCGTCATGGAGTTGGACGCCTGCGC-3′. Using Gibson assembly, the three PCR products were inserted into the SpeI site of the MiniMos vector pCFJ909 (a gift from Erik Jorgensen; Addgene plasmid no. 44480), which harbors the *cb-unc-119*(+) rescue fragment. Microinjection of the obtained plasmid pBC1918 (10 ng/μl) into the strain HT1593[*unc-119(ed3)*] using MiniMos (Frøkjær-Jensen et al., 2014) generated the single-copy insertion allele *bcSi118*. To label the peroxisomal membrane with GFP, the *GFP::linker::pxmp-4* construct was generated by fusion PCR (as indicated above for the *mKate2::linker::pxmp-4* construct). This construct was then amplified using the primers 5′-AAAAATATTGTTCCAGAAAAATGA GTAAAGGAGAAGAAC-3′ and 5′-TTAAATTATTCCGTTTTTATTTGGATGGAATTCGAATAG-3′. The *mKate2::linker::daf-22* fragment of the plasmid pBC1918 was replaced by the *GFP::linker::pxmp-4* PCR product using Gibson assembly. Microinjection of the obtained plasmid pBC1945 (10 ng/μl) into the strain HT1593[*unc-119(ed3)*] using MiniMos (Frøkjær-Jensen et al., 2014) generated the single-copy insertion *bcSi119*. To generate a reporter strain expressing *daf-22p::mKate2::linker::daf-22* and *daf-22p::GFP::linker::pxmp-4*, the strains MD4635 (*bcSi118*) and MD4666 (*bcSi119*) were crossed.

METHOD DETAILS

RNA interference experiments

RNAi by feeding was performed using bacterial clones from the Ahringer library (Kamath and Ahringer, 2003), with the exception of *acox-1.1(RNAi)*, which was taken from the Vidal library (Rual et al., 2004) and *tag-208(RNAi)* (Rolland et al., 2019). *tag-208(RNAi)* did not induce the *lonp-2p::GFP* and *ctl-2p::GFP* reporters expression as compared to empty vector *mock(RNAi)* (Figure S7). *tag-208(RNAi)* was therefore used in this study as a negative control and was referred to as *control(RNAi)*. The *acox-1.6(RNAi)* clone was generated by amplification of the first three exons of *acox-1.6* from genomic DNA using the primers 5′-ATCATCGATGAATT CGAGCTCATGAGTCGATGGATTCAGC-3′ and 5′-CTATAGGGCGAATTGGGTACCTTGAAGTGTTGGAATAAACATAAC-3′. The PCR product was inserted into the SacI KpnI site of pPD129.36 (a gift from Andrew Fire; Addgene plasmid no. 1654) by Gibson assembly. The obtained plasmid was transformed into HT115 RNAi bacteria. On day one, the RNAi clones were cultured overnight at 37°C and 200 rpm in 2 mL of LB carbenicillin (100 μg/ml) tetracycline (12.5 μg/ml). On day two, 20 μL of the overnight culture was used to inoculate 2 mL of LB carbenicillin (100 μg/ml) and further grown at 37°C and 200 rpm for 6 hours. The 6 hours RNAi cultures were adjusted to 0.5OD and 50 μL was used to seed a first set of 30 mm RNAi plates (NGM medium (Stiernagle, 2006) supplemented with 100 μg/ml carbenicillin and 6 mM IPTG). *prx-5(RNAi)* was diluted 1:2 with *control(RNAi)* to reduce slow growth phenotype. The plates were incubated in the dark at room temperature until the next day. On day three, four to eight L4 larvae of the *hsp-6p::GFP*, *lonp-2p::GFP* or *ctl-2p::GFP* reporter strains were inoculated onto the seeded RNAi plates and incubated at 20°C for 22 h. In addition, a second set of RNAi plates were seeded (following the same protocol as for the first set of RNAi plates) on day three. On day four, the four to eight adults were transferred onto the second set of RNAi plates, let to lay eggs for four hours at 20°C and then removed. The plates were incubated for three days at 20°C. For each RNAi condition, about 10-15 F1 gravid adults were mounted on 2% agarose pads, immobilized with 1 mM Levamisol and imaged using a Leica GFP dissecting microscope (M205 FA) and the software Leica Application Suite (3.2.0.9652).

In the case of the RNAi experiment to analyze the peroxisomal number, no lay-off was done to synchronize the population. Instead, F1 animals were mounted on 2% agarose pads and the stage was determined by DIC microscopy. Only young adults carrying not more than three eggs were imaged using a Zeiss Axioskop 2 (100x, NA 1.3) and the MetaMorph software (7.1.0.0) (Molecular Devices) or a Leica SP5 confocal microscope (HCX PL APO Lambda Blue 63x 1.4 oil objective) and the LAS AF software (Leica).

To generate samples for RT-qPCR, the RNAi experiment was carried out as described above with following changes: 20 L4 larvae of the wild-type strain N2 and 60 L4 larvae of the *lonp-2p::GFP* or *ctl-2p::GFP* reporter strains were treated by RNAi on 30 mm RNAi plates and let to lay eggs onto 60 mm RNAi plates on the following day. Adult animals of the next generation were washed off the plates with 1.5 mL MPEG and collected in cryogenic tubes. The worm pellet was washed three times with 1ml MPEG. The worm pellet was resuspended in 1 mL TRIzol Reagent (Invitrogen), flash frozen in liquid nitrogen and stored at −80°C.

The protocol was also modified for the preparation of the samples for the RNA-seq and lipidomic analysis. The experiment was carried out on 100 mm RNAi plates containing 6 mM IPTG that were seeded with 600 μL of the RNAi cultures. In order to reduce the slow-growth phenotype, the *prx-5(RNAi)* culture was diluted 1:2 (vol/vol) with *mock(RNAi).* About 160 N2 L4 larvae were pipetted onto each RNAi plate (two plates per condition) and the next day a lay-off for 2 h at 20°C was performed on a second set of RNAi plates. The synchronized progeny was incubated for three days (*tag-208(RNAi)*) or four days (*prx-5(RNAi)*) at 20°C to reach the adult stage and then collected in a tube. The worm pellet was first washed with 50ml MPEG. The pellet was transferred into a 1.5 mL eppendorf tube and washed two times with 1 mL of MPEG and two times with 1 mL of M9. The samples were flash frozen in liquid nitrogen and stored at −80°C until they were analyzed.

For the preparation of the samples for the proteomic analysis, the RNAi by feeding protocol was also modified. The RNAi clones were streaked out on LB carbenicillin (100 μg/ml) tetracycline (12.5 μg/ml) plates on day one and the plates were incubated overnight at 37°C. On day two, the RNAi bacteria were resuspended in LB and the OD was adjusted to 0.5. A first set of 100 mm RNAi plates (same protocol as above) were seeded with 600 μL of RNAi culture. The *prx-5(RNAi)* RNAi culture was diluted 1:2 (vol/vol) with mock (HT115 RNAi bacteria containing the empty RNAi vector pPD129.36) in order to reduce the slow-growth phenotype. On day three, two seeded RNAi plates per condition were each inoculated with ∼200 N2 L4 larvae and incubated at 20°C for 22 h. In addition, a second set of RNAi plates were seeded (following the same protocol as for the first set of RNAi plates) on day three. On day four, the gravid adults were transferred onto the second set of RNAi plates, let to lay eggs for four hours at 20°C and then removed. The plates were incubated for three days (mock and *tag-208(RNAi)*) or four days (*prx-5(RNAi)* diluted 1:2) at 20°C. The gravid adults were collected in a tube and the worm pellet was washed four times with 10 mL of 1x PBS. The samples were flash frozen in liquid nitrogen and stored at −80°C until they were analyzed by mass spectrometry.

Protein quantification

Proteins were extracted and digested using the iST Preomics Kit (Germany) with an initial step of sonication with glass beads (Bioruptor, Diagenode).

For the mass spectrometry analysis, 5 μl were injected in an RSLCnano system (Thermo) and separated in a 25-cm analytical Aurora C18 nanocolumn (75 μm ID 120 Å, 1.6 μm, Ion Opticks) with a 120-min gradient from 4 to 40% acetonitrile in 0.1% formic acid. The effluent from the HPLC was directly electrosprayed into a Q Exactive HF (Thermo). The Q Exactive HF instrument was operated in data dependent mode to automatically switch between full scan MS and MS/MS acquisition. Survey full scan MS spectra

(from m/z 375–1600) were acquired with resolution R = 60000 at m/z 400 (AGC target of $3x10^6$). The ten most intense peptide ions with charge states between 3 and 5 were sequentially isolated to a target value of $1x10^5$ and fragmented at 27% normalized collision energy with R = 15000. Typical mass spectrometric conditions were: spray voltage, 1.5 kV; no sheath and auxiliary gas flow; heated capillary temperature, 250°C; ion selection threshold, 33.000 counts.

MaxQuant 1.5.2.8 was used to identify proteins and quantify by LFQ with the following parameters: Database, Uniprot_3AUP000001940_Celegans-; MS tol, 10ppm; MS/MS tol, 10ppm; Peptide FDR, 0.1; Protein FDR, 0.01 Min. peptide Length, 5; Variable modifications, Oxidation (M); Fixed modifications, Carbamidomethyl (C); Peptides for protein quantitation, razor and unique; Min. peptides, 1; Min. ratio count, 2. Identified proteins were considered as up/down-expressed if their MaxQuant LFQ values displayed a log2 value > 1 or < −1 and a p value of 0.05 in a limma moderated t test adjusted for multiple comparisons when compared to the control.

RT-qPCR

The worm pellet in TRIzol (Invitrogen) was thawed and total RNA was extracted after three freeze-thaw cycles with liquid nitrogen/37°C heat block following the manufacturer's instructions (Invitrogen). The RNA was purified using the RNeasy Mini Kit (QIAGEN) including an on-column DNase I digest (QUIAGEN) and the quantity and quality was determined using a NanoPhotometer (IMPLEN) and agarose gel electrophoresis. cDNA was synthesized from 600 ng RNA using the ProtoScript II First Strand cDNA Synthesis Kit (NEB) with Oligo-dT primers. Quantitative PCR was performed in three technical replicates per biological cDNA sample using a CFX96 Real-Time PCR Detection System with the CFX Maestro Software (BioRad). Each reaction contained diluted cDNA (1:4 vol/vol) or nuclease free water as control, iTaq Universal SYBR Green Supermix (BioRad) and 400 nM of gene-specific primers (Table S5). Cycling conditions were set as following: Initial denaturation for 30 s at 95°C, followed by 40 cycles of 5 s at 95°C and 30 s at 60°C. The melt curve was analyzed for 60 cycles of 5 s per 0.5°C increment. Technical replicates were averaged and relative expression to one of the RNAi control samples was calculated using the ΔΔCt method (Livak and Schmittgen, 2001) with *cdc-42* as reference gene (Hoogewijs et al., 2008). For visualization, the mean of the relative expression for the control RNAi condition was normalized to 1. Therefore, the mean and standard deviation within one gene were divided by the mean of the control sample of the respective gene.

RNA-seq analysis

RNA-seq was performed by Eurofins Genomics Europe Shared Services GmbH. Total RNA was extracted using commercial kits with modified and optimized protocols. The library was prepared with an optimized protocol and standard Illumina adaptor sequences have been used. Sequencing was performed with Illumina technology, HiSeq 4000 (read mode 1 × 50bp). The bioinformatics analysis included the alignment of the RNA-seq reads to the reference genome using Bowtie (Langmead et al., 2009). Cufflinks, Cuffmerge and Cuffdiff was used to determine the differential expression levels. Genes were considered as significantly changed with an FDR < 0.05 after Benjamini-Hochberg correction for multiple testing.

Lipidomic analysis

Lipids were extracted using the BUME method (Löfgren et al., 2012). Briefly, worms were resuspended in 50 μL MeOH and transferred to custom made bead beating tubes. Samples were homogenized at 8000 rpm in a Precellys Bead Beater for 3 times 10 s with 20 s breaks in between. The additional Cryolys module was used with liquid nitrogen to prevent excessive heating of samples during disruption. 150 μL butanol and 200 μL heptane-ethyl acetate (3:1) was added to each sample sequentially which were then incubated for 1 h at 500 rpm / RT. 200 μL 1% acetic acid was added to each sample followed by centrifugation for 15 min at 13000 rpm / 4°C. The upper organic phase was transferred to a fresh Eppendorf tube and the lower aqueous phase was re-extracted by the addition of 200 μL heptane-ethyl acetate followed by incubation and centrifugation as described above. The upper organic phase was transferred to the already obtained organic phase. The lower phase was transferred to a new Eppendorf tube and used for metabolomic analyses. Samples were evaporated to dryness and stored at −20°C. For lipidomics, samples were re-dissolved in 50 μL 65% isopropanol/ 35% acetonitrile/ 5% H2O, vortexed and 40 μL were transferred to an autosampler vial. The remaining 10 μL were pooled to form a QC sample for the entire study. The precipitated proteins in the aqueous phase were used for determination of protein content using a Bicinchoninic Acid Protein Assay Kit (Sigma-Aldrich, Taufkirchen, Germany).

Lipids were analyzed as previously described. Briefly, lipids were separated on a Waters Acquity UPLC (Waters, Eschborn, Germany) using a Waters CORTECS UPLC C18 column (150 mm x 2.1 mm ID, 1.6 μm particle size, Waters, Eschborn Germany) and a linear gradient from eluent A (40% H2O / 60% ACN + 10 mM ammonium formate / 0.1% formic acid) to eluent B (10% ACN / 90% iPrOH + 10 mM ammonium formate / 0.1% formic acid). The following gradient was used: 68/32 at 0min, 68/32 at 1.5min, 3/97 at 21min, 3/97 at 25 min, 68/32 at 25.1 min with a flow rate of 0.250 ml/min and a temperature of 40°C. Mass spectrometric detection was performed using a Bruker maXis UHR-ToF-MS (Bruker Daltonic, Bermen, Germany) in positive ionization mode using data dependent acquisition to obtain MS1 and MS2 information. Negation ionization mode data was recorded for identification of lipids. Every six samples, a pooled QC was injected to check performance of the UPLC-UHR-ToF-MS system and were used for normalization.

Raw data was processed with Genedata Expressionist for MS 13.5 (Genedata AG, Basel, Switzerland). Preprocessing steps included noise subtraction, m/z recalibration, chromatographic alignment and peak detection and grouping. Data was exported

for Genedata Expressionist for MS 13.5 Analyst statistical analysis software and as .xlsx for further investigation. Maximum peak intensities were used for statistical analysis and data was normalized on the protein content of the sample and an intensity drift normalization based on QC samples was used to normalize for the acquisition sequence.

Lipid features that were detected in all pooled QC samples and had a relative standard deviation (RSD) < 30% were further investigated by statistical analysis. Comparison of *prx-5(RNAi)* versus *control(RNAi)* was performed using a Welch test. Lipids with a p value < 0.05 were considered to be significantly changed.

Lipids were putatively annotated on the MS1 level using an in-house developed database for *C. elegans* lipids and bulk composition from LipidMaps (113), when available. Matching of MS2 spectra against an in-silico database of *C. elegans* lipids and LipidBlast was performed using the masstrixR package (Kind et al., 2013; Kind et al., 2014) (M.W., unpublished data; https://github.com/michaelwitting/masstrixR) and only hits with a forward and reverse matching score > 0.75 were considered. Annotations of interesting biological peaks were manually verified and corrected if necessary.

Analysis of the effect of PA14 infection on the expression of the PRS reporters

Pseudomonas aeruginosa PA14 killing plates were prepared as previously described (Powell and Ausubel, 2008). The *lonp-2p::GFP*, *ctl-2p::GFP, daf-22p::GFP* reporter strains were synchronized by bleaching. Synchronized L1 larvae were inoculated on NGM plates with *E. coli* strain OP50 as a food source and cultured at 25°C until the young adult stage. Worms were harvested in a 15 ml falcon tube and washed three times with 50 mM NaCl. Half of the worms were transferred to PA14 killing plates, the other half to an NGM plate with OP50. Plates were dried briefly under a laminar flow hood and then incubated at 25°C for 4, 8 or 24 hours before being harvested in 50 mM NaCl. GFP expression of reporter strains was quantified with the COPAS (Complex Object Parametric Analyzer and Sorter) Biosort system (Union Biometrica; Holliston, MA) as described in Pujol et al. (2008). For each strain, a minimum of 150 synchronized young adult worms were analyzed for length (assessed as TOF, time of flight), optical density (assessed as extinction) and green fluorescence (GFP). Raw data were filtered on the TOF for adult worms (typically $300 \leq TOF \leq 1500$). The ratio GFP/TOF is represented in arbitrary units.

Image analysis and image representation

The analysis of two-dimensional images using Fiji/ImageJ2 (Rueden et al., 2017; Schindelin et al., 2012) was automated by a Fiji-implemented macro using the IJ1 Macro language. The analysis of the *hsp-6p::GFP*, *lonp-2p::GFP* or *ctl-2p::GFP* reporter strains was performed as previously described (Rolland et al., 2019). For the analysis of the peroxisomal number, the background of the fluorescent images was subtracted with a rolling ball radius of five pixels. Next, a binary mask of the image was generated using the Otsu automated threshold. The mask was inverted and noise was removed by applying the Particle Analyzer with a minimum size of four pixels. The mask was multiplied with the original image and the number of peroxisomes was measured by the 3D Objects counter plug-in for ImageJ.

The representative images in the main figures were set using the following approach. For each reporter strain in a given Figure, the maximum pixel intensity of the image was measured for the control (max(control)). The minimum displayed value of the images was set to 0 and the maximum displayed value was set to max(control). It should be noted that since the strongest induction in all representative images was 2-fold, some of the pixels in these images are therefore saturated. In Figure S3, we show the same images as in the main Figures but the maximum displayed value is set to 2*max(control). In this case, none of the pixels in the image are saturated.

QUANTIFICATION AND STATISTICAL ANALYSIS

Statistical analysis was performed using the software R (3.6.1) (R Core Team, 2017). Normal distribution of the data was tested by a Shapiro-Wilk test and by the analysis of diagnostic plots. Equal variance was tested using an F-test if two independent groups were compared and a Brown-Forsythe test if more than two independent groups were compared. If the data showed normal distribution and equal variance, a two sample t test was applied to compare two independent groups. In the case of heteroscedasticity, a Welch two sample t test was used and in the case of not normally distributed data, a Mann-Whitney-U test was used. For the comparison of more than two groups, heteroscedastic and non-parametric data was analyzed using a Kruskal-Wallis test with Dunns's multiple comparison and Holm's p value adjustment. Data showing a normal distribution and equal variance was analyzed using a one-way ANOVA with Dunnett's multiple comparison.